30 Years Working with Jaffre and Roberts on Modeling Flow in Porous Media

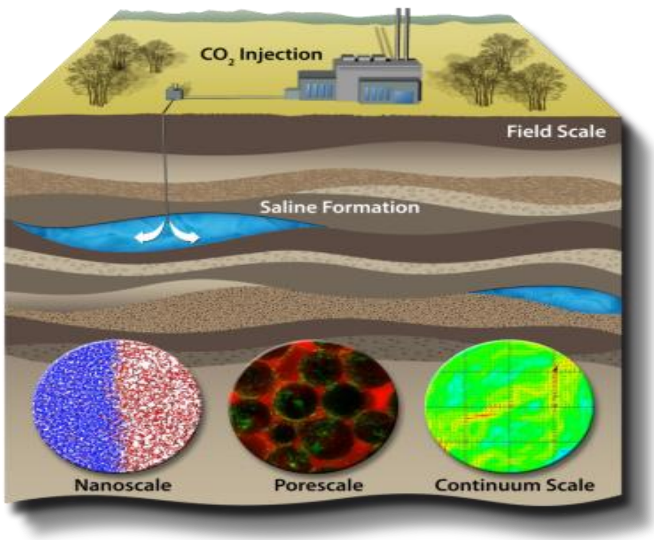

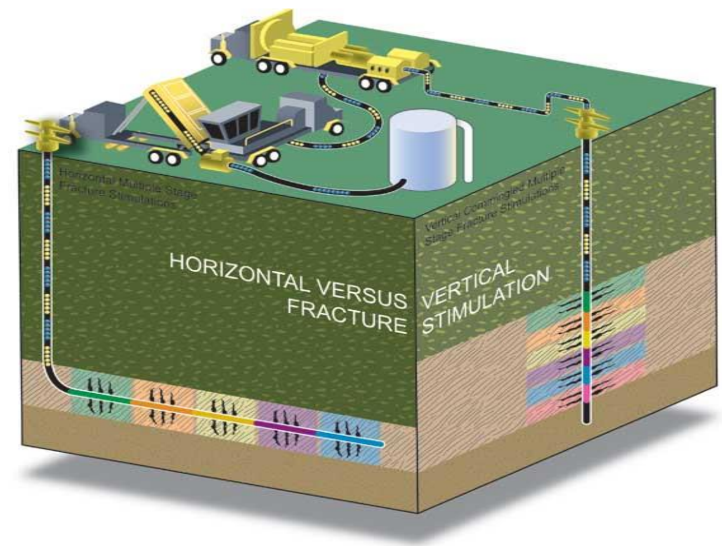

Mary F. Wheeler
ICES Center for Subsurface Modeling
The University of Texas at Austin

Center for Subsurface Modeling

Selected Jaffre/ Roberts Computational Research Contributions

- **Book: Mathematical Models and Finite Elements for Reservoir Simulation: Single Phase , Multiphase and Multicomponent Flows through Porous Media, Chavent and Jaffre (1986)**
- **Mixed and Hybrid Methods, Roberts and Thomas, (1991)**
- **Upstream Weighting and Mixed Finite Elements in Simulation of Miscible Displacements, Jaffre and Roberts (1983)**
- **On Upstream Mobility Schemes for 2-Phase Flow in Porous Media, Mishra and Jaffre**
- **Decomposition for Flow in Porous Media with Fractures (1999)**
- **Modeling Fractures and Barriers as Interfaces for Flow in Porous Media, Martin, Jaffre, Roberts(2005)**
- **-Godunov Type Methods for Conservation Laws with a Flux Function Discontinuous in Space**

Societal Needs in Relation to Geological Systems

Resources Recovery
- Petroleum and natural gas recovery from conventional/unconventional reservoirs
- *In situ* mining
- Hot dry rock/enhanced geothermal systems
- Potable water supply
- Mining hydrology

Site Restoration
- Aquifer remediation
- Acid-rock drainage

Waste Containment/Disposal
- Deep waste injection
- Nuclear waste disposal
- CO_2 sequestration
- Cryogenic storage/petroleum/gas

Underground Construction
- Civil infrastructure
- Underground space
- Secure structures

Acknowledge

Mojdeh Delshad, Changli Yuan,
Andro Mikelic, Ivan Yotov,
Thomas Wick, Gergina Pencheva,
Vivette Girault, Kundan Kumar,
Gurpreet Singh.

Jaffre/ Roberts: Mixed Methods, Multiphase Flow, Reactive Transport, Miscible Displacement and Fingering, DG, Fracture Modeling,

Outline (Work Motivated by Jaffre/Roberts)

- Multipoint Flux Mixed Finite Element Method (MFMFE) for Flow and Coupling with Geomechanics
  - Example: poroelasticity with fixed fractures
- Chemical EOR: Polymer Flow and ASP (alkaline, surfactant, polymer)
- EOS Compositional Flow
  - Formulation
  - Brugge Co2 EOR
  - Coupling with EnKF for In Salah Co2 Sequestration
- Conclusions

Single Phase Flow

$$
\begin{aligned}
\mathbf{u} &= -K\nabla p && \text{in } \Omega, \\
\nabla \cdot \mathbf{u} &= f && \text{in } \Omega, \\
p &= 0 && \text{on } \partial\Omega,
\end{aligned}
$$

$$
\begin{aligned}
(K^{-1}\mathbf{u}_h, \mathbf{v})_Q - (p_h, \nabla \cdot \mathbf{v}) &= 0, && \forall \mathbf{v} \in V_h \\
(\nabla \cdot \mathbf{u}_h, q) &= (f, q), && \forall q \in W_h
\end{aligned}
$$

- Q represents the quadrature rule

Corner Point Geometry - Highly Distorted Hexahedra

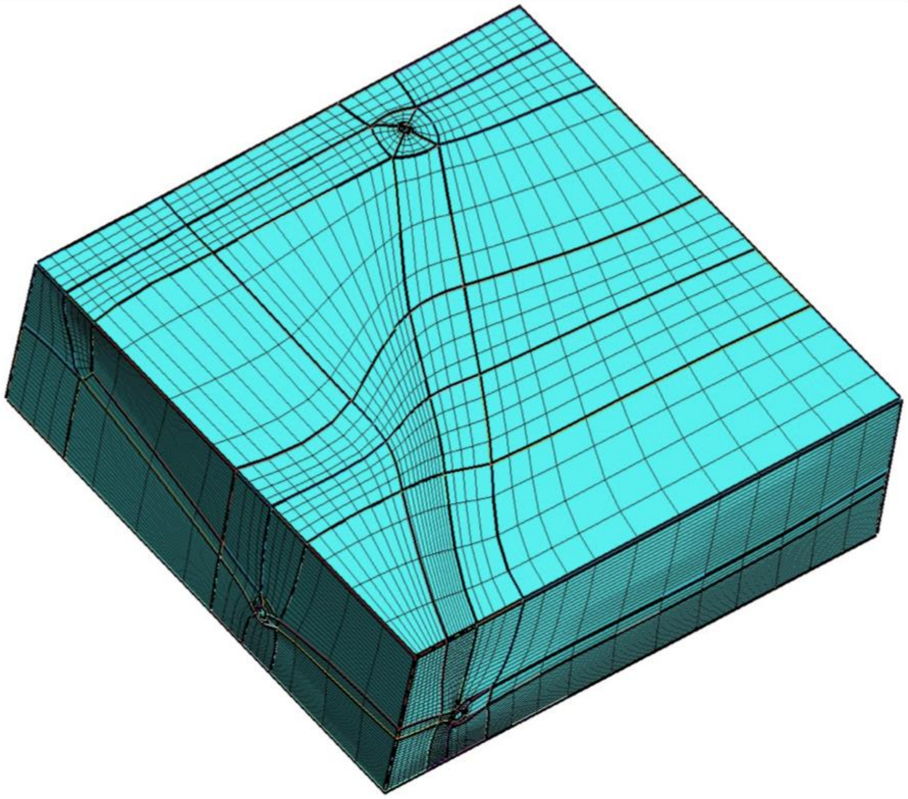

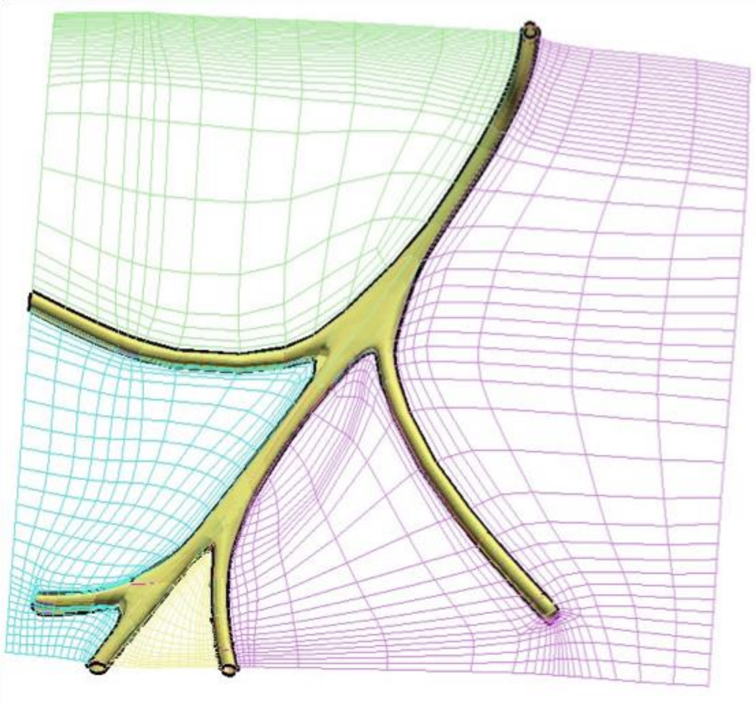

Multipoint Flux Mixed Finite Element

- Provably accurate:
- Pressure to second order;
- Velocity to first order.
- Locally mass conservative.
- Easy to implement.
- Current Extensions:
- Non-isothermal compositional model.
- Nonplanar fractured grids.

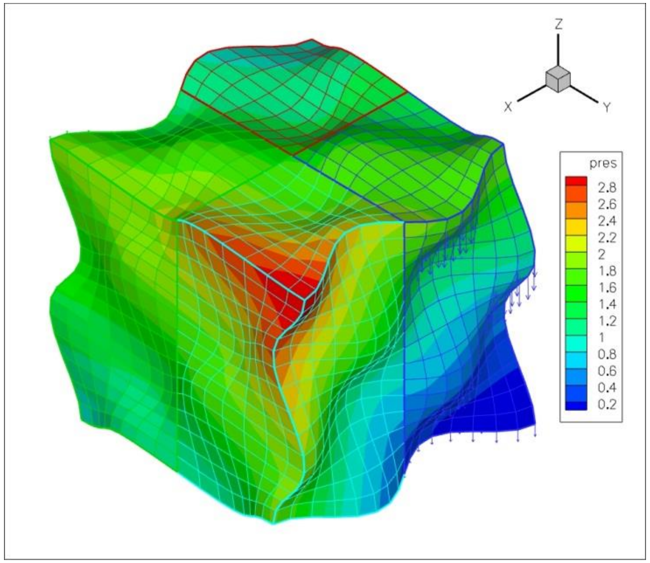

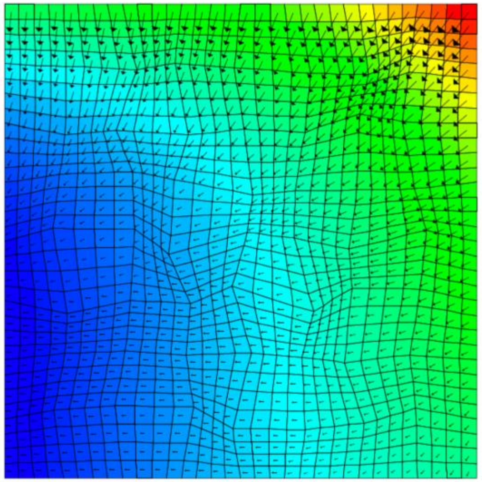

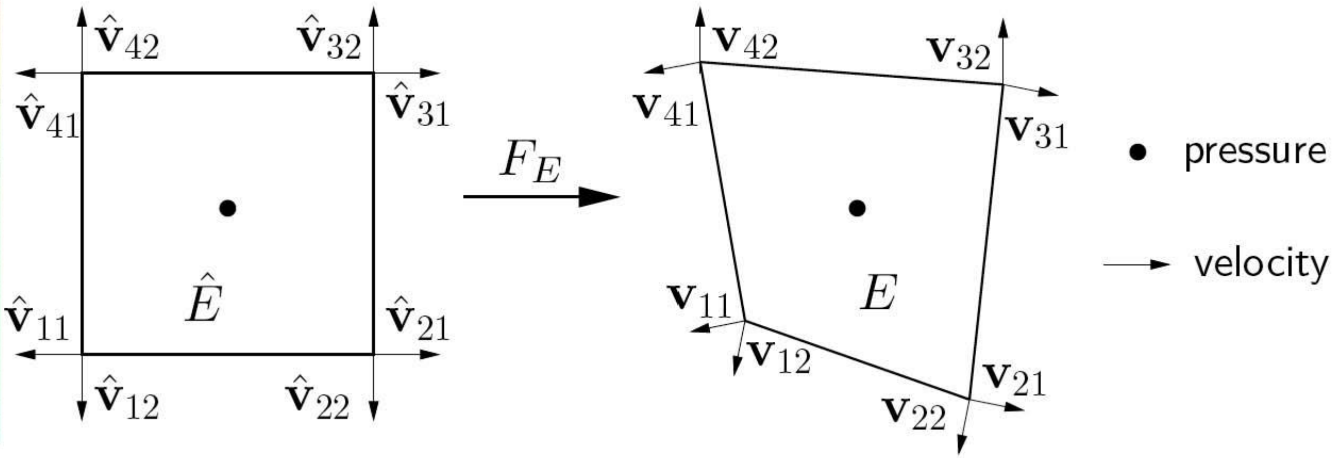

Fractured Reservoir Flow Model

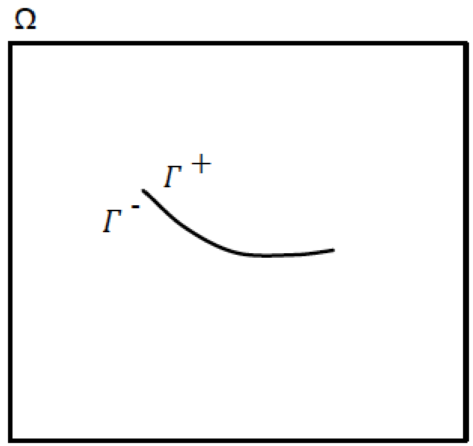

- Interface as pressure specified BC for reservoir
- No-flow BC for fracture
- Jump in reservoir flux across interface as the source term for fracture

Model Formulation

Reservoir Flow

$$\frac{\partial}{\partial t}\left(\phi^* S_\beta \rho_\beta\right) + \nabla \cdot \boldsymbol{z}_\beta = q_\beta$$

$$\boldsymbol{z}_\beta = -\boldsymbol{K} \rho_\beta \frac{k_{r\beta}}{\nu_\beta}\left(\nabla p_\beta - \rho_\beta \boldsymbol{g}\right)$$

Fracture Flow

$$\frac{\partial}{\partial t}\left(w S_\beta^\Gamma \rho_\beta^\Gamma\right) + w \bar{\nabla} \cdot \boldsymbol{z}_\beta^\Gamma = q_\beta^\Gamma + q_{l\beta}$$

$$\boldsymbol{z}_\beta^\Gamma = -\boldsymbol{K}^\Gamma \rho_\beta^\Gamma \frac{k_{r\beta}}{\nu_\beta}\left(\bar{\nabla} p_\beta^\Gamma - \rho_\beta^\Gamma \boldsymbol{g}\right)$$

Interface Conditions

$$\boldsymbol{z}_\beta \cdot n = 0 \text{ on } \partial\Omega^N$$

$$p_{\text{ref}} = p^D \text{ on } \partial\Omega^D$$

$$S_{\text{ref}} = S^D \text{ on } \partial\Omega^D$$

$$p_{\text{ref}} = p^D \text{ on } \Gamma^\pm$$

$$S_{\text{ref}} = S^D \quad \text{ on } \Gamma^\pm$$

$$q_{l\beta} = [\boldsymbol{z}_\beta \cdot \boldsymbol{n}]^\Gamma = \boldsymbol{z}_\beta \cdot \boldsymbol{n}|_{\Gamma-} - \boldsymbol{z}_\beta \cdot \boldsymbol{n}|_{\Gamma+}$$

$$w = [\boldsymbol{u} \cdot \boldsymbol{n}]^\Gamma = \boldsymbol{u} \cdot \boldsymbol{n}|_{\Gamma-} - \boldsymbol{u} \cdot \boldsymbol{n}|_{\Gamma+}$$

$$\boldsymbol{K}^\Gamma = \frac{w^2}{12}$$

Coupling Reservoir and Fracture Flow

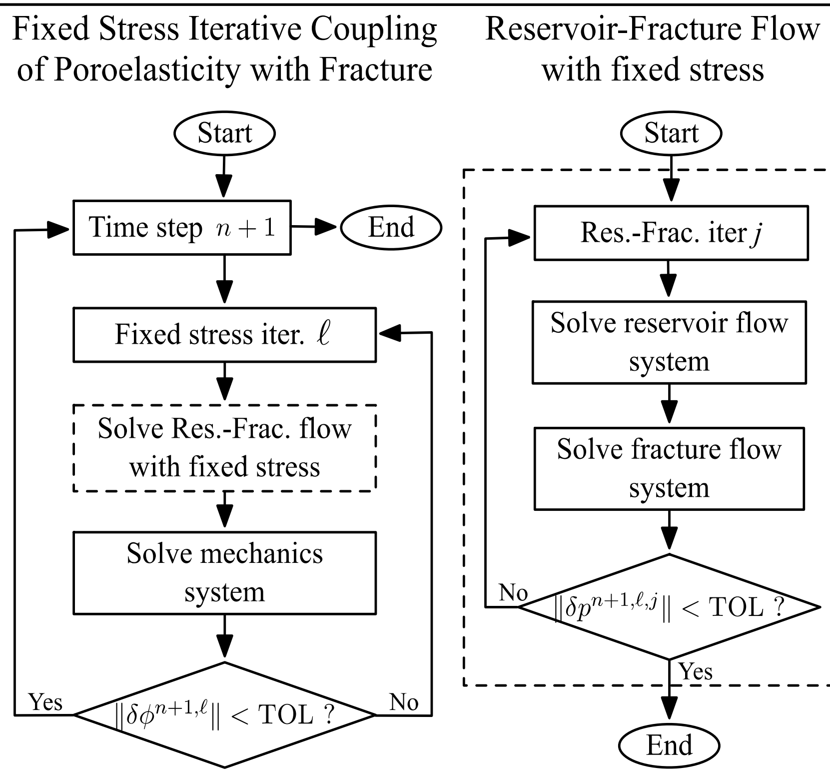

- **Coupling of standard Biot of linear poroelasticity and flow (iterative coupling—Mikelic ,W) in fracture governed by lubrication (Kumar, W)**
- **Theorem**: Existence and uniqueness and a priori results established for coupled linearized system under weak assumptions on data. Error estimates also derived. (Girault, W, Ganis, Mear)

A Lubrication Fracture Model in a Poro-Elastic Medium

- Darcy's Law (reservoir flow), Linear Elasticity (reservoir mechanics), and Reynold's Lubrication (fracture flow).

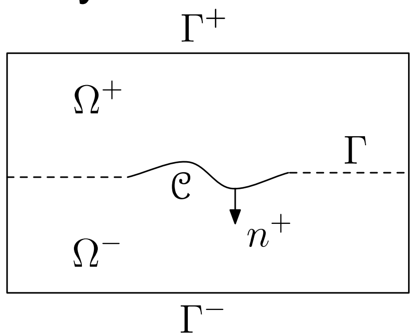

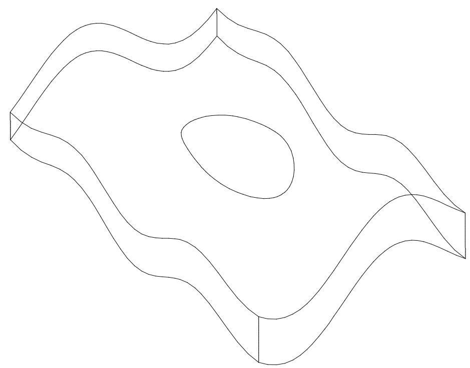

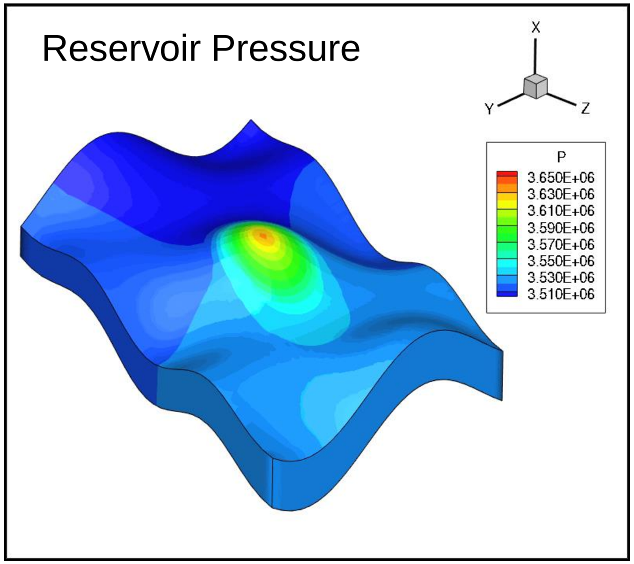

- Multipoint flux mixed finite elements on hexahedra.

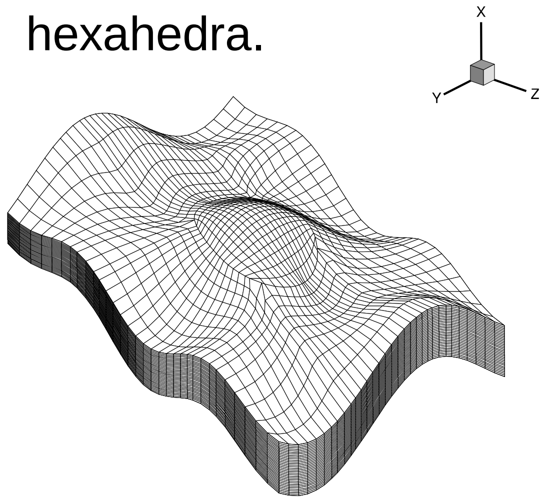

- Solution algorithm uses iterative coupling.

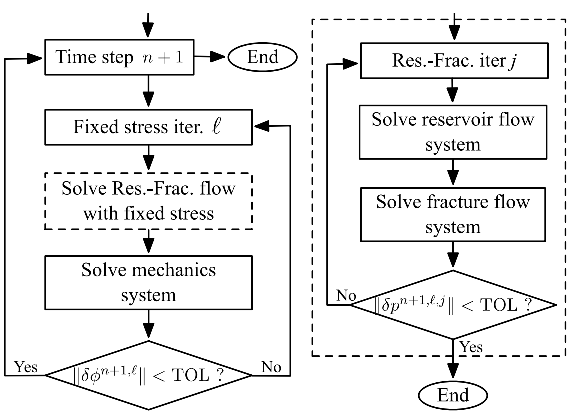

- Unknowns include width, leakoff, traction.
- Existence and uniqueness were proven.
- Has been extended to multiphase flow in IPARS.

Center for Subsurface Modeling

Motivation for Chemical EOR Studies

- ✓ Improve oil recovery efficiency for displacements with unfavorable mobility ratio and very heterogeneous reservoirs
- ✓ Target bypassed oil left after waterflood
- ✓ Reduce mobility ratio to improve areal and vertical sweep efficiencies
- ✓ Compare efficiency/accuracy of different numerical schemes (IMPES, IMPLICIT, Iterative Coupling, Time splitting)
- ✓ Process scale up to field scale
- ✓ Chemical EOR in fractured porous media, e,g, Alaska

Improved Mobility & Sweep Efficiency

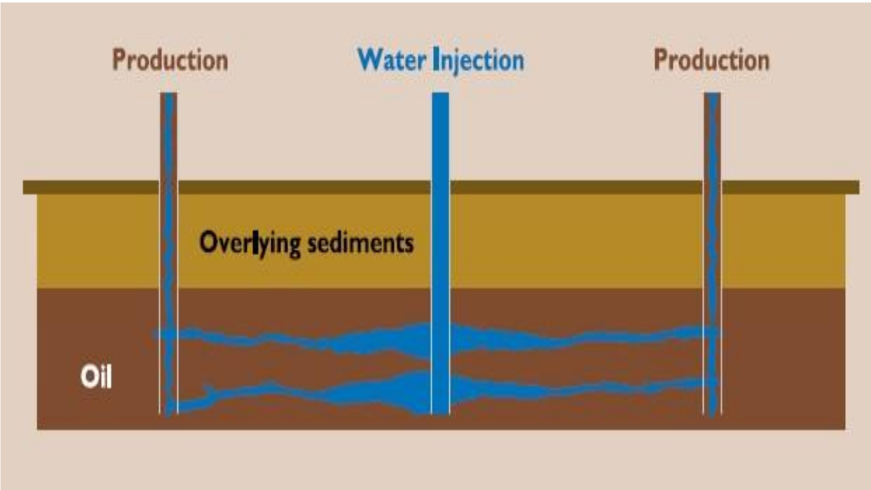

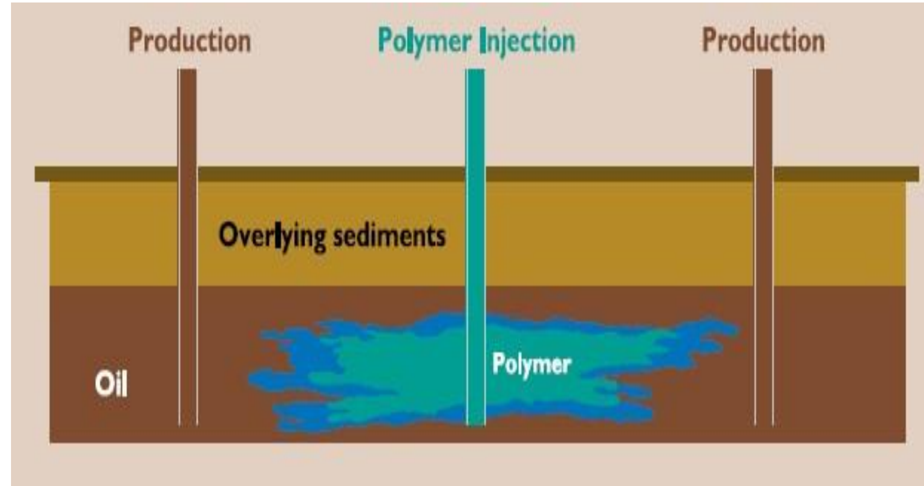

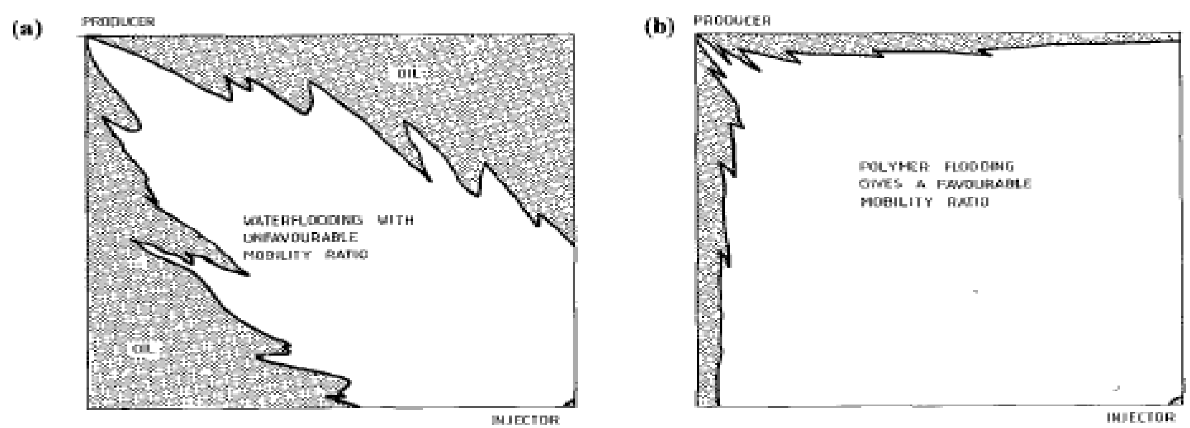

Figure 8.2. Schematic diagram of the improvement of areal sweep caused by polymer flooding in a five-spot system.

Center for Subsurface Modeling

Polymer Structure

Large chains of repeating monomers linked by covalent bonds

Xanthan (MW ~ 2- 50 MM)

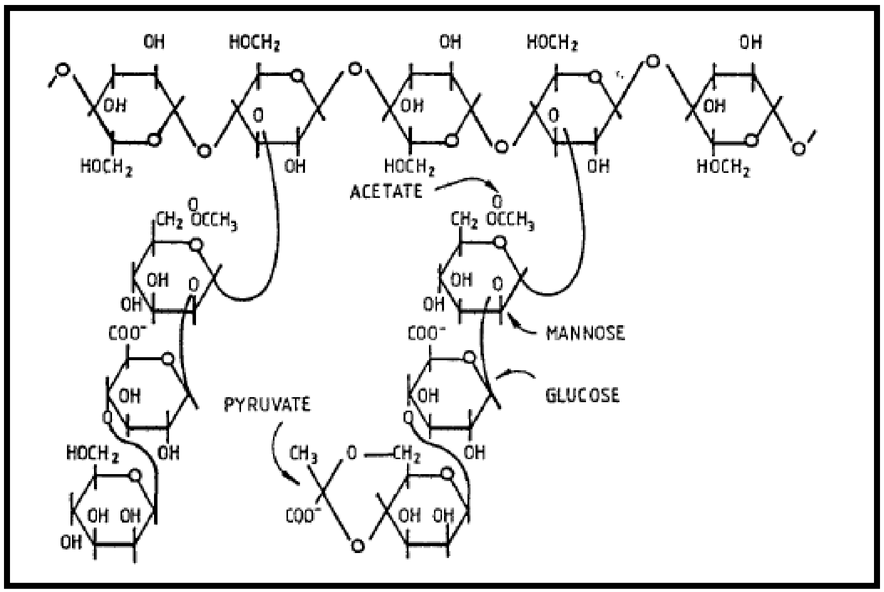

Polyacrylamide (MW ~ 2- 30 MM)

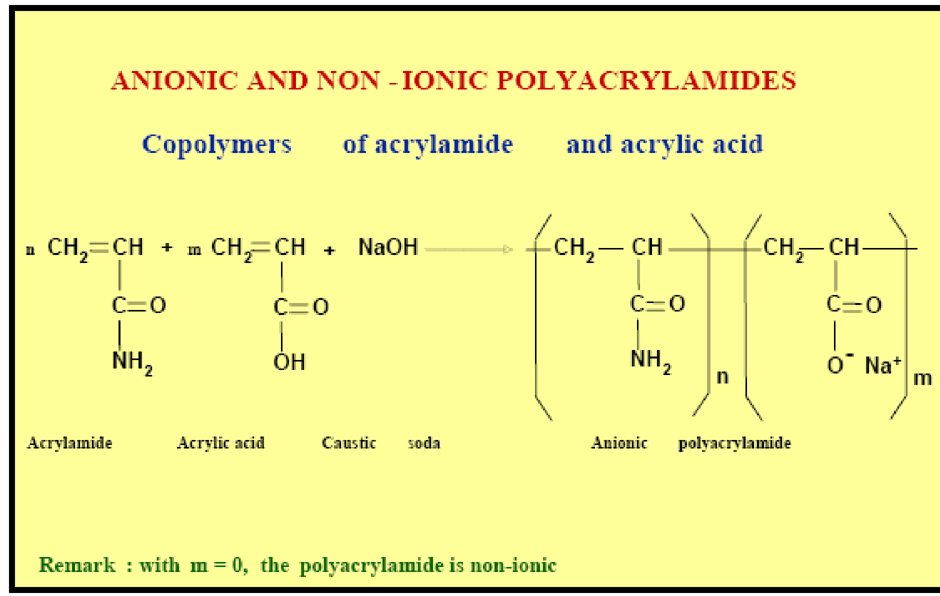

Mobility Ratio

The ratio of displacing fluid mobility to displaced fluid mobility:

$$M = \frac{\lambda_w}{\lambda_o} = \frac{k_w / \mu_w}{k_o / \mu_o} = \frac{k_w \mu_o}{k_o \mu_w}$$

$M \leq 1$ Piston-like displacement

Small amount of polymer increases water viscosity

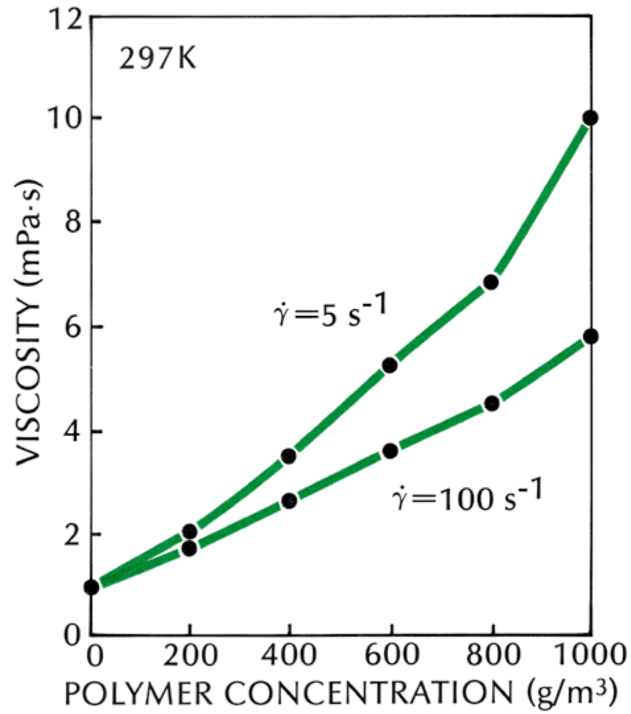

Source: Lake, 1989

Center for Subsurface Modeling

Polymer Rheology

Dilute polymer solutions are pseudoplastic (shear thinning)

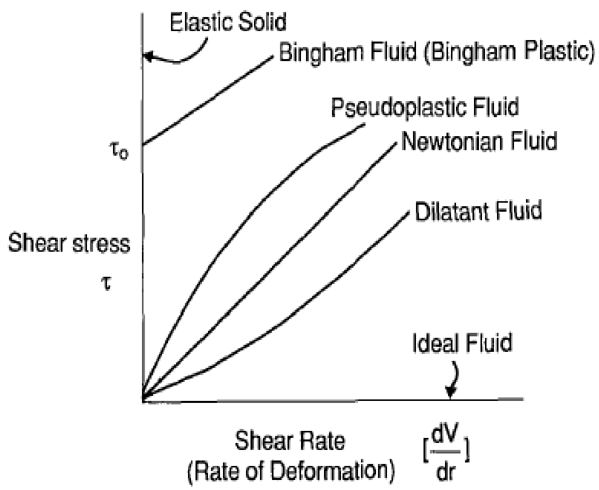

Figure 3.5. Different types of shear stress/shear rate behaviour found in polymeric fluids; the elastic solid and ideal fluid cases are also shown.

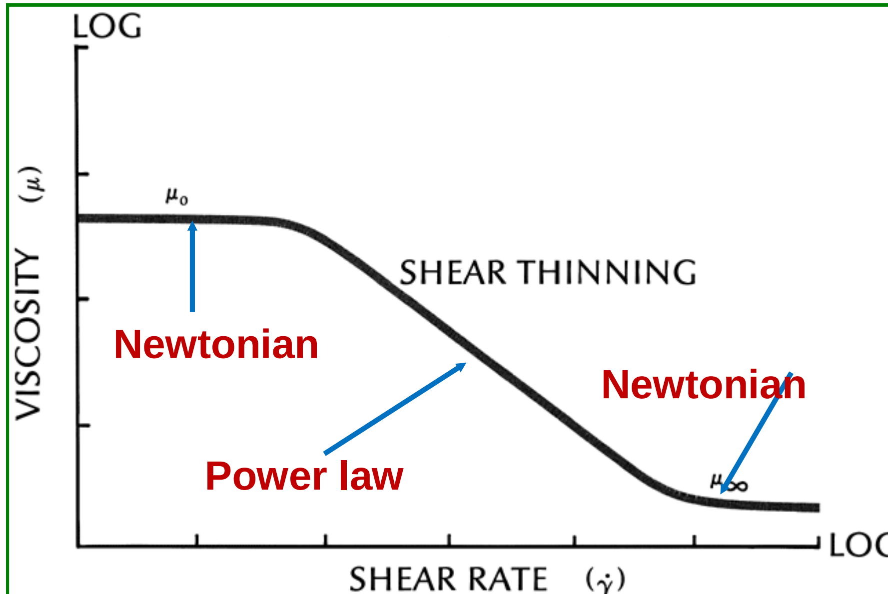

IPARS-TRCHEM

- Two phase oil/water
- Compressible fluids
- MFMFE Based
- Time split method for flow and concentration (transport, diffusion/ dispersion)
- Non-differentiable inequality constraints – model as minimization of Gibbs free energy using interior pt.
- Several boundary condition options
- Wells as volumetric or pressure constraint
- AMG solver with pre-conditioner
- Parallel computation capability
- General geochemistry and biochemistry modules

Polymer Properties in IPARS-TRCHEM

- ✓ Viscosity as a function of
  - Concentration
  - Salinity
  - Shear rate
- ✓ Adsorption
- ✓ Permeability reduction
- ✓ Inaccessible pore volume

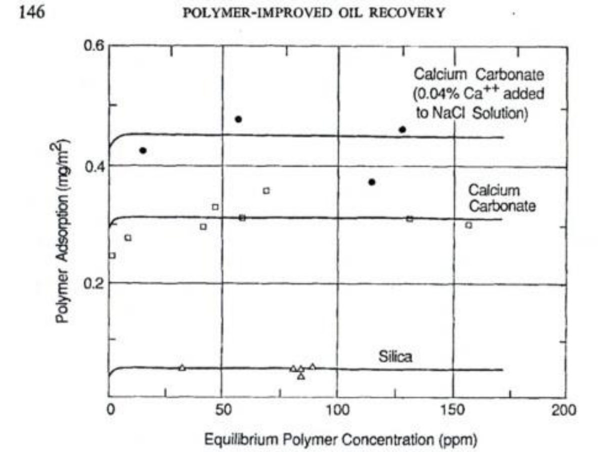

Figure 5.9. Adsorption isotherms for HPAM (M) from 10% sodium chloride solution onto calcium carbonate and silica substrates (after Smith, 1970).

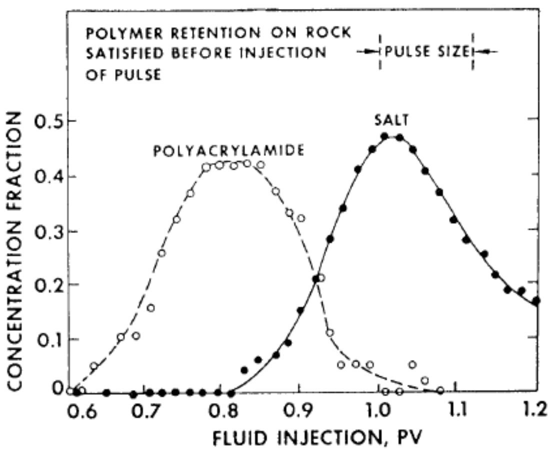

Figure 7.9. Original experimental demonstration of the inaccessible pore volume phenomenon using HPAM and salt (from Dawson and Lantz, 1972).

Chemical Flooding Modules

- Surfactant
  - Reduce the interfacial tension between oil and water phases
  - Target bypassed oil left after waterflood by mobilizing oil trapped in pores due to capillary pressure/force

- Polymer
  - Reduce water mobility to improve areal and vertical sweep efficiencies
  - Target bypassed oil left after waterflood due to unfavorable mobility ratio and heterogeneity

- Model field-scale tests using parallel computation

Multiphase Flow Equations

- Mass Conservation for each phase

$$\frac{\partial(\phi\rho_\alpha S_\alpha)}{\partial t} + \nabla\cdot\left(\rho_\alpha \mathbf{u}_\alpha\right) = q_\alpha$$

- Darcy's Law: $\mathbf{u}_\alpha = -\frac{k_\alpha}{\mu_\alpha}\mathbf{K}(\nabla p_\alpha - \rho_\alpha g \nabla z)$

- Saturation constraint: $\sum_\alpha S_\alpha = 1$

- Capillary pressure: $P_c(S_w) = P_n - P_w$

Reactive Species Transport Model

- Mass balance of species *i* in phase *α* :

$$\frac{\partial(\phi c_{i\alpha} S_\alpha)}{\partial t} + \nabla \cdot (c_{i\alpha}\vec{u}_\alpha - \phi S_\alpha \vec{\vec{D}}_{i\alpha} \nabla c_{i\alpha}) = \phi S_\alpha R^C_{i\alpha} + q_{i\alpha}$$

- An equilibrium linear partition between phases

$$c_{i\alpha} = \Gamma_{i\alpha} c_{ir}$$

- Phase-summed species transport equation:

$$\frac{\partial(\phi_i^* c_{iw})}{\partial t} + \nabla \cdot (c_{iw}\vec{u}_i^* - \vec{\vec{D}}_i^* \nabla c_{iw}) = q_i^T + R_i^{TC}$$

$$\phi_i^* = \phi(S_w + \Gamma_{io} S_o) \qquad \vec{u}_i^* = \vec{u}_w + \Gamma_{io}\vec{u}_o \qquad q_i^T = q_w + \Gamma_{io} q_o$$

$$\vec{\vec{D}}_i^* = \phi(S_w \vec{\vec{D}}_{iw} + S_o \Gamma_{io} \vec{\vec{D}}_{io}) \qquad R_i^{TC} = \phi(S_w R^C_{iw} + S_o R^C_{io})$$

Component Transport Equations

- Mass balance of species *i* in phase *α* :

$$\frac{\partial(\phi c_{i\alpha} S_\alpha)}{\partial t} + \nabla \cdot c_{i\alpha} u_\alpha - \phi S_\alpha D_{i\alpha} \nabla c_{i\alpha} = q_{i\alpha}$$

- The diffusion-dispersion tensor $D_{i\alpha}$ is given by:

$$\mathbf{D}_{i\alpha} = \mathbf{D}_{i\alpha}^{\mathrm{mol}} + \mathbf{D}_{i\alpha}^{\mathrm{hyd}}$$

$$\mathbf{D}_{i\alpha}^{\mathrm{hyd}} = f(velocity)$$

Validation against an IMPES Code

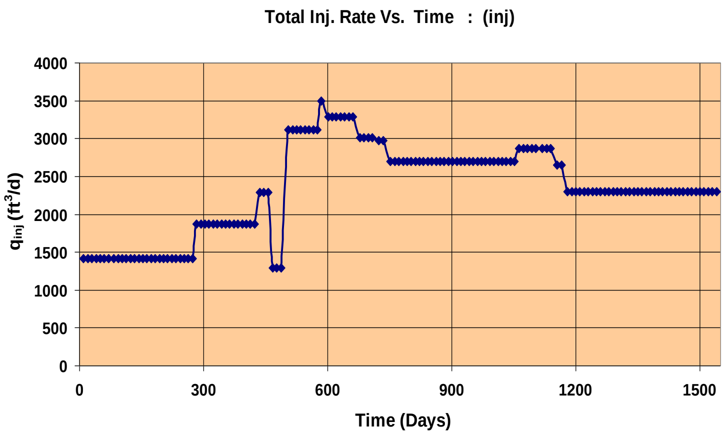

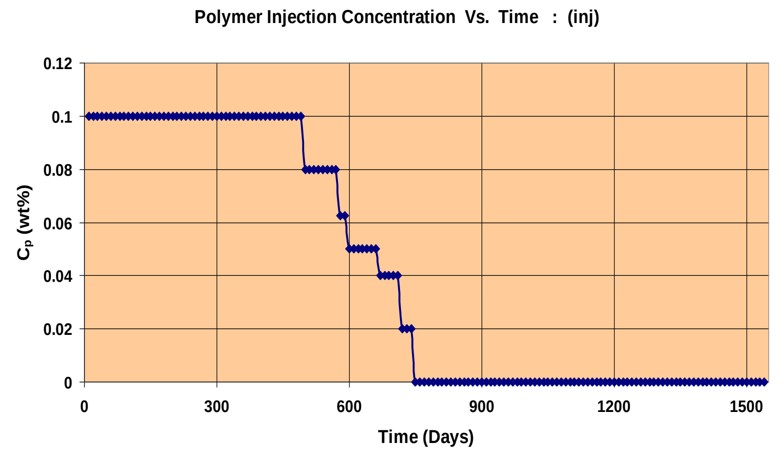

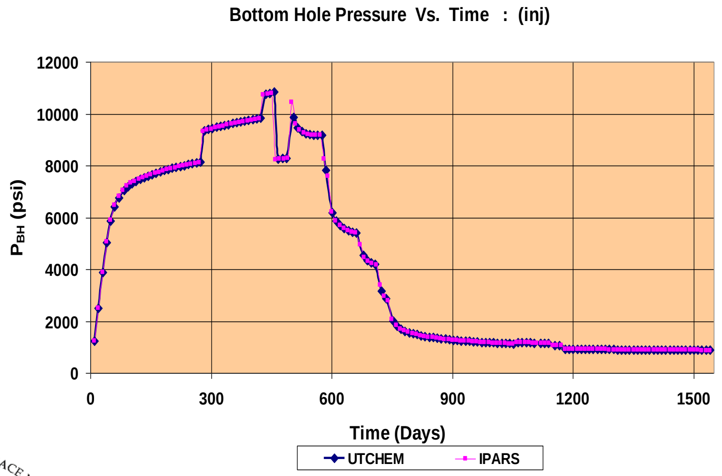

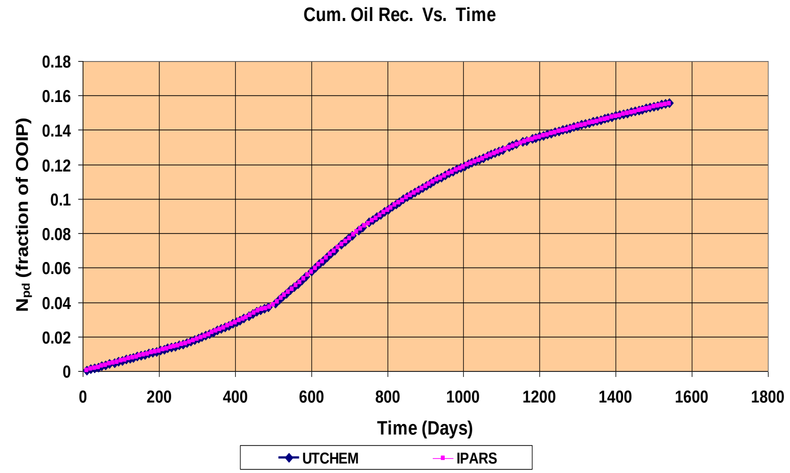

Parallel Simulation of Polymer Injection

- 200 cp oil viscosity (endpoint mobility ratio = 107)
- Domain size : 10240 ft x 5120 ft x 160 ft
- Grid size: 20 ft x 10 ft x 10 ft
- No. of gridblocks : 4,194,304
- Average perm. : (about 10 D)
- 32 five spots with 37.6 acre well patterns
- 32 injection wells and 45 production wells
- Constant pressure injection (below parting pressure)
- 128 processors

Polymer Flood Simulations

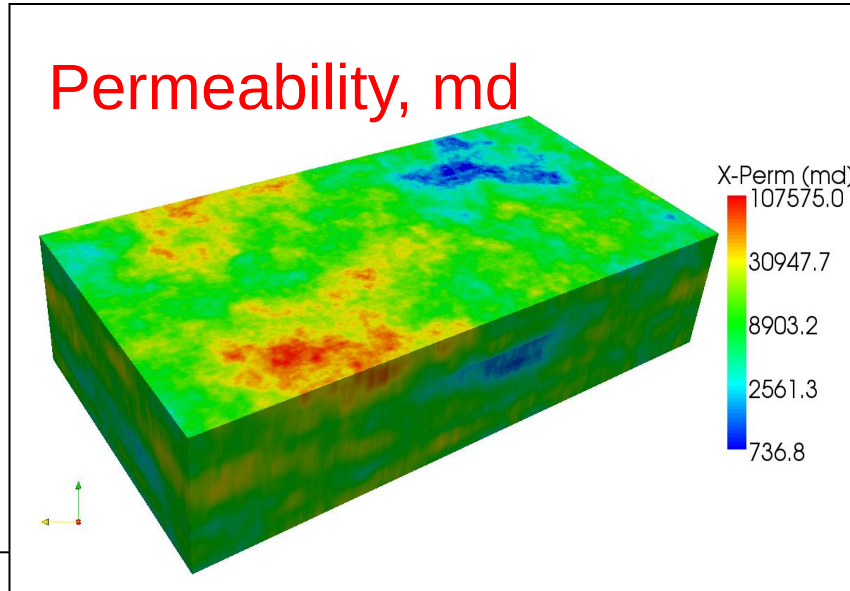

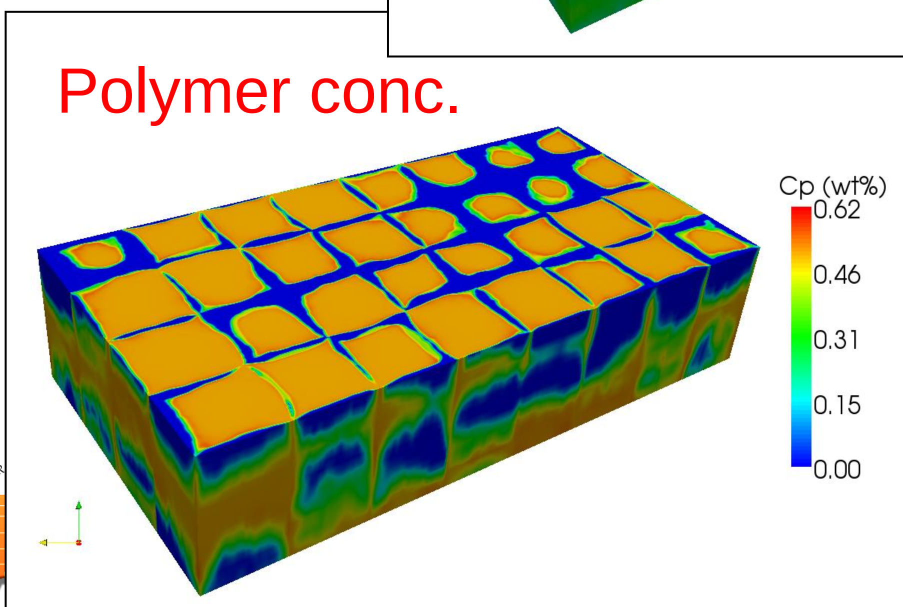

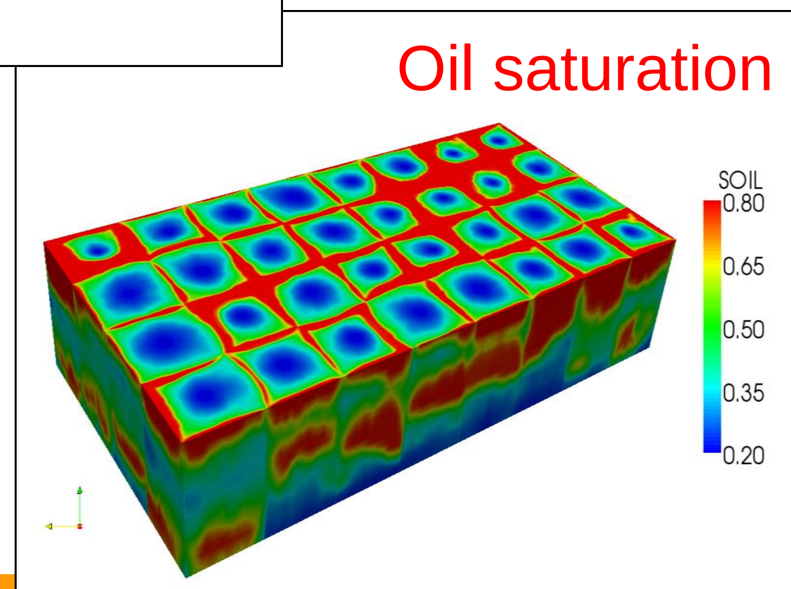

Polymerflood Recovery for Viscous Oil

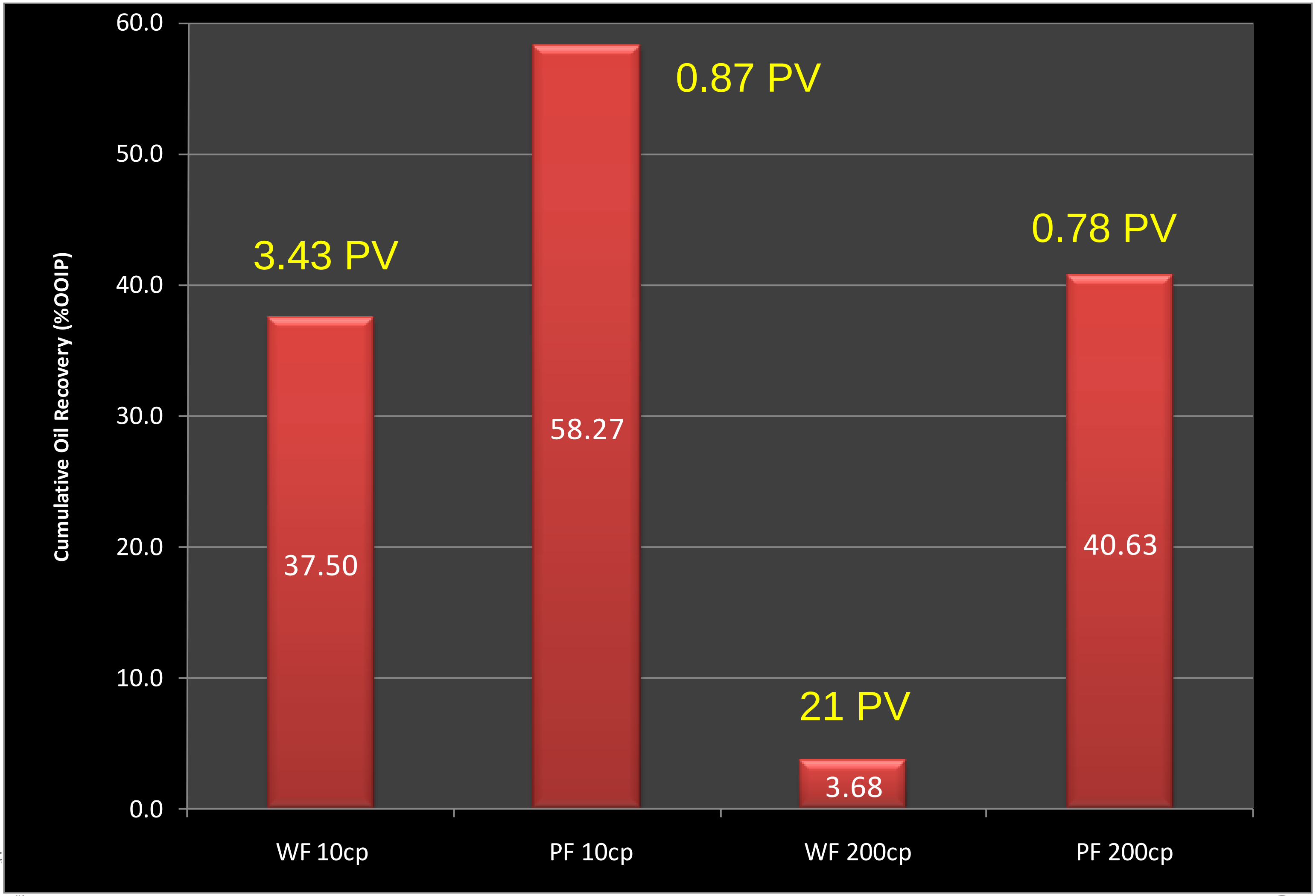

2000 days

4000 days

Center for Subsurface Modeling

Parallel Scalability

CPU Time

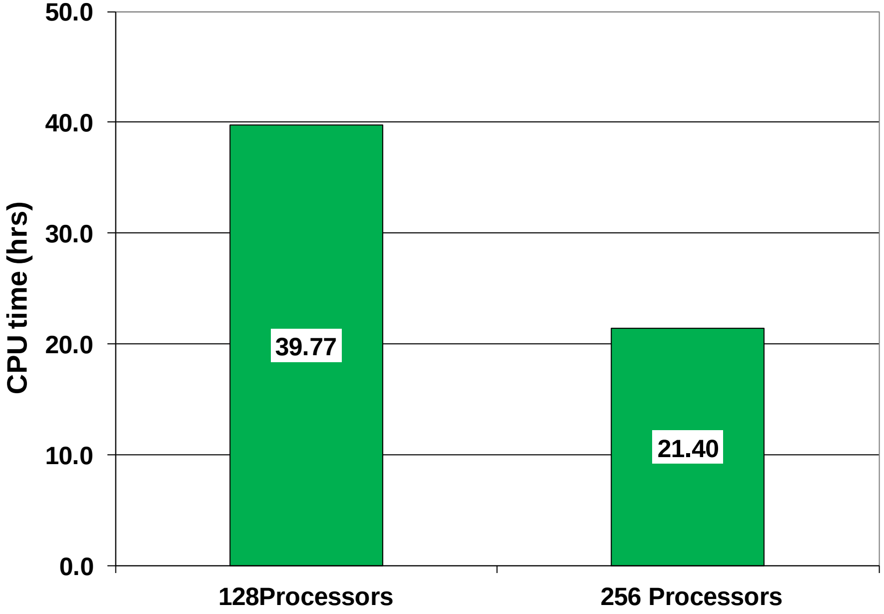

Parallel Scalability

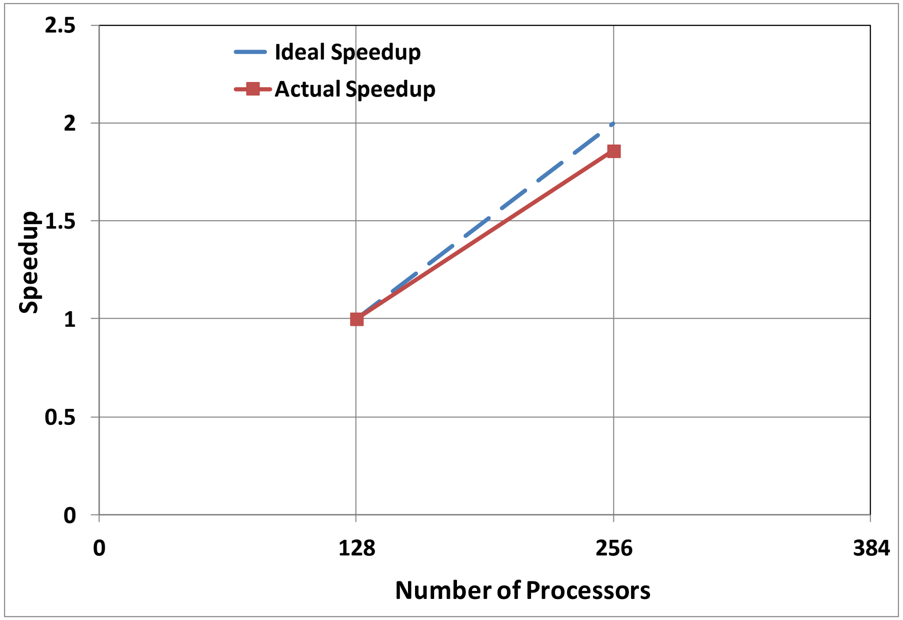

ASP Model Species

Polymer flood: 3+ species, the first 3 species must be polymer, anion (Cl^-), cation (Ca^{2+})

SP flood: 4+ species, the first 4 species must be polymer, anion (Cl^-), cation (Ca^{2+}), surfactant

ASP flood: 12+ species, the first 12 species must be polymer, anion (Cl^-), cation (Ca^{2+}), surfactant, H^+, HA_o, CO_3^{2-}, Na^+, Mg^{2+}, A^-, HA_w, OH^-

Alkaline/Surfactant/Polymer (ASP) Flood Flowchart

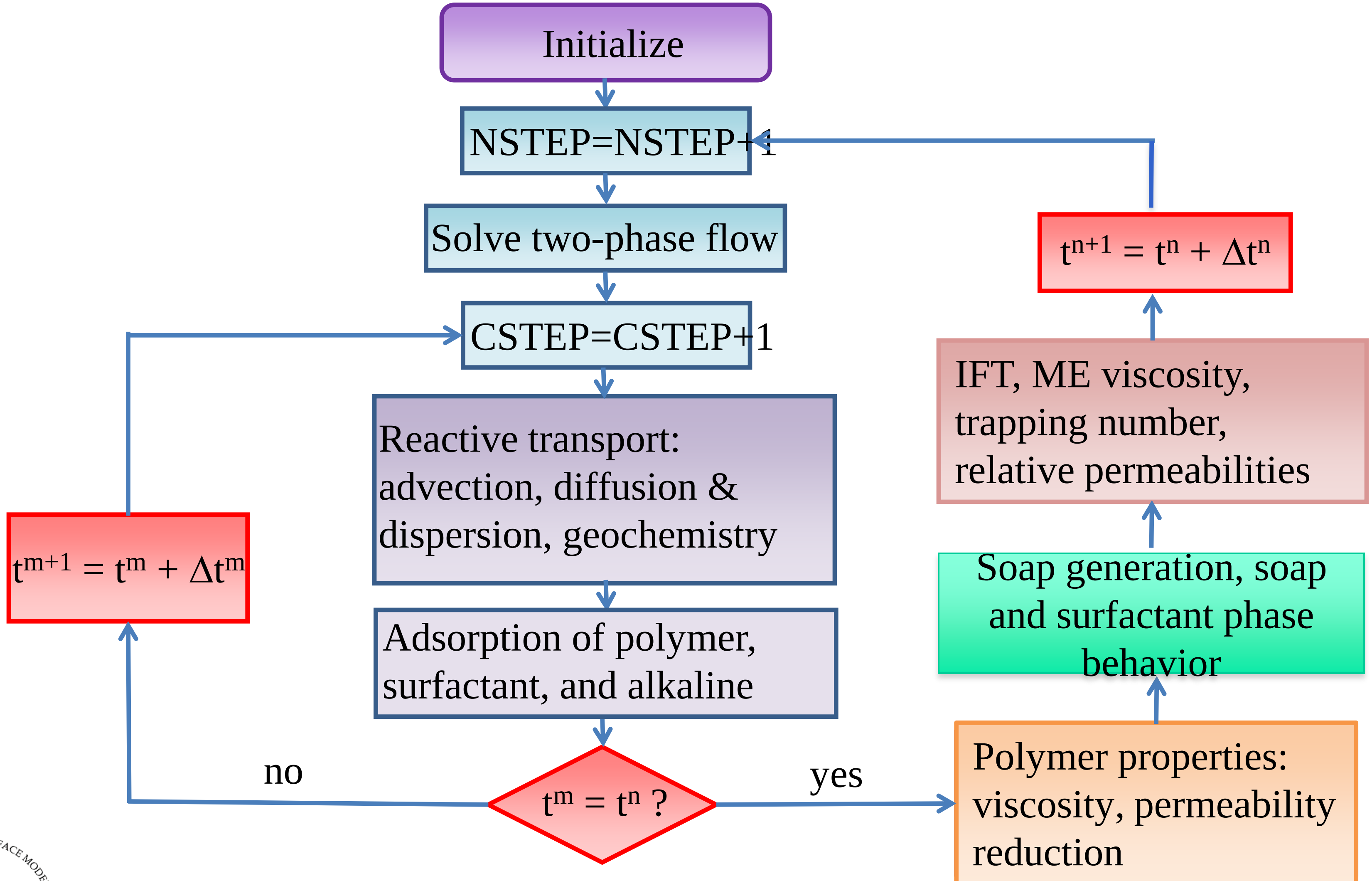

Alkaline/Surfactant/Polymer Module Features

- Polymer, surfactant, and alkaline adsorptions
- Non-Newtonian polymer solution and micoremulsion (ME) viscosities
- Permeability reduction and pore volume reduction
- In situ generation of soap by reaction of alkaline with the acid in crude oil
- Phase behavior as a function of soap and surfactant concentrations
- Aqueous geochemical reactions, mineral dissolution/precipitation, and ion exchange with clays in the rock and micelles

Field-scale unstable polymer flood

- Reservoir dimensions: 1024 x 256 x 256 (ft)
- Gridblocks in each direction: 128 x 64 x 128
- Gridblock sizes: 8 x 4 x 2 (ft)
- Total gridblocks: 1,048,576
- Number of processors : 64
- Simulation time: 100 Day

Field-scale unstable polymer flood (Cont.)

- Average permeability: 2100md
- Porosity: 0.23
- Oil viscosity: 2000cp
- 1 horizontal injector at the bottom with P_{BH}= 15000psi
- 1 horizontal producer at the top with P_{BH}= 3000psi
- Injection rate: about 2600~3000STB/Day
- Injected polymer conc.: 0.07497lbmol/ft^3 (0.12wt%)

Polymer Viscosity

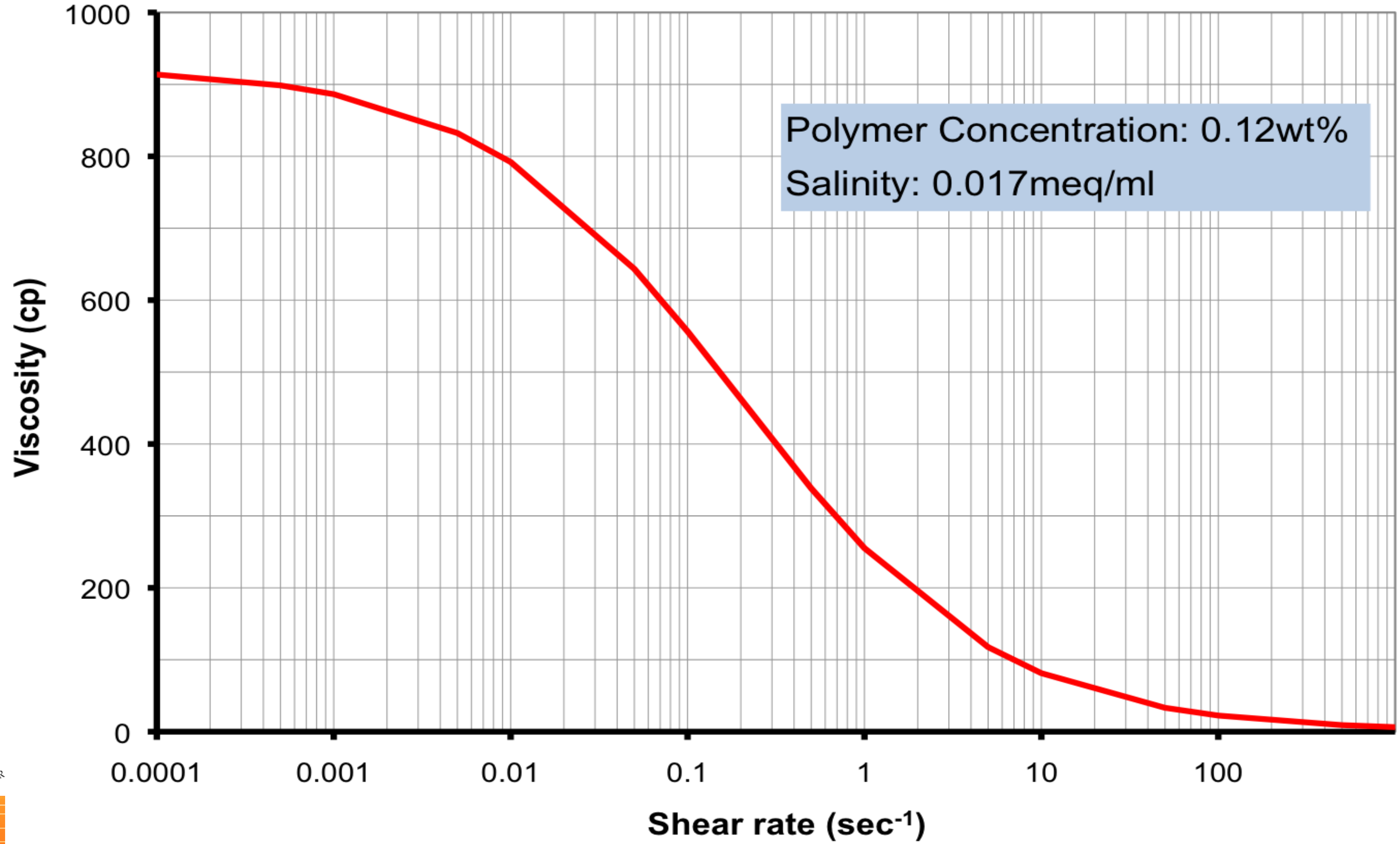

Relative Permeabilities

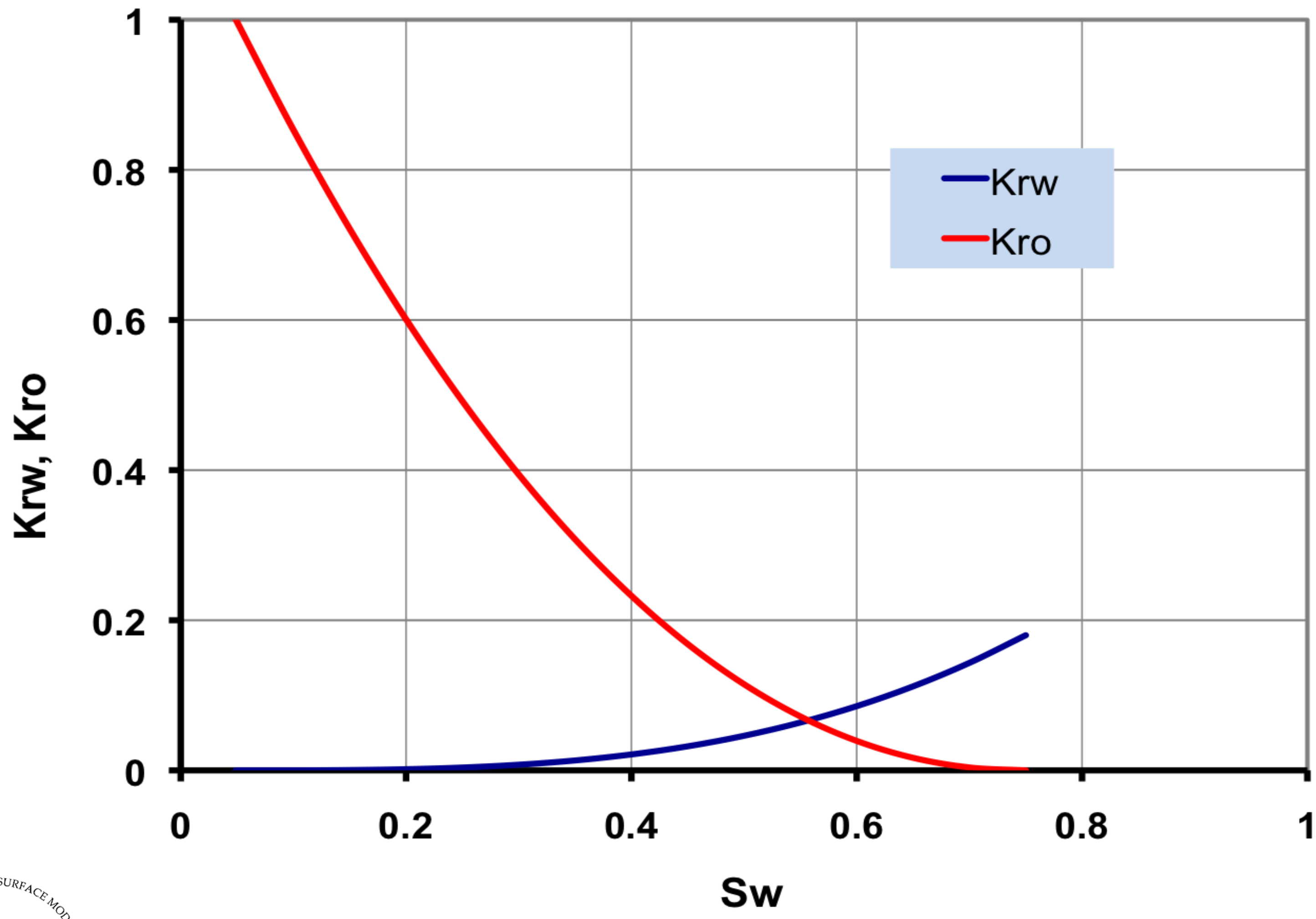

Relative Permeabilities

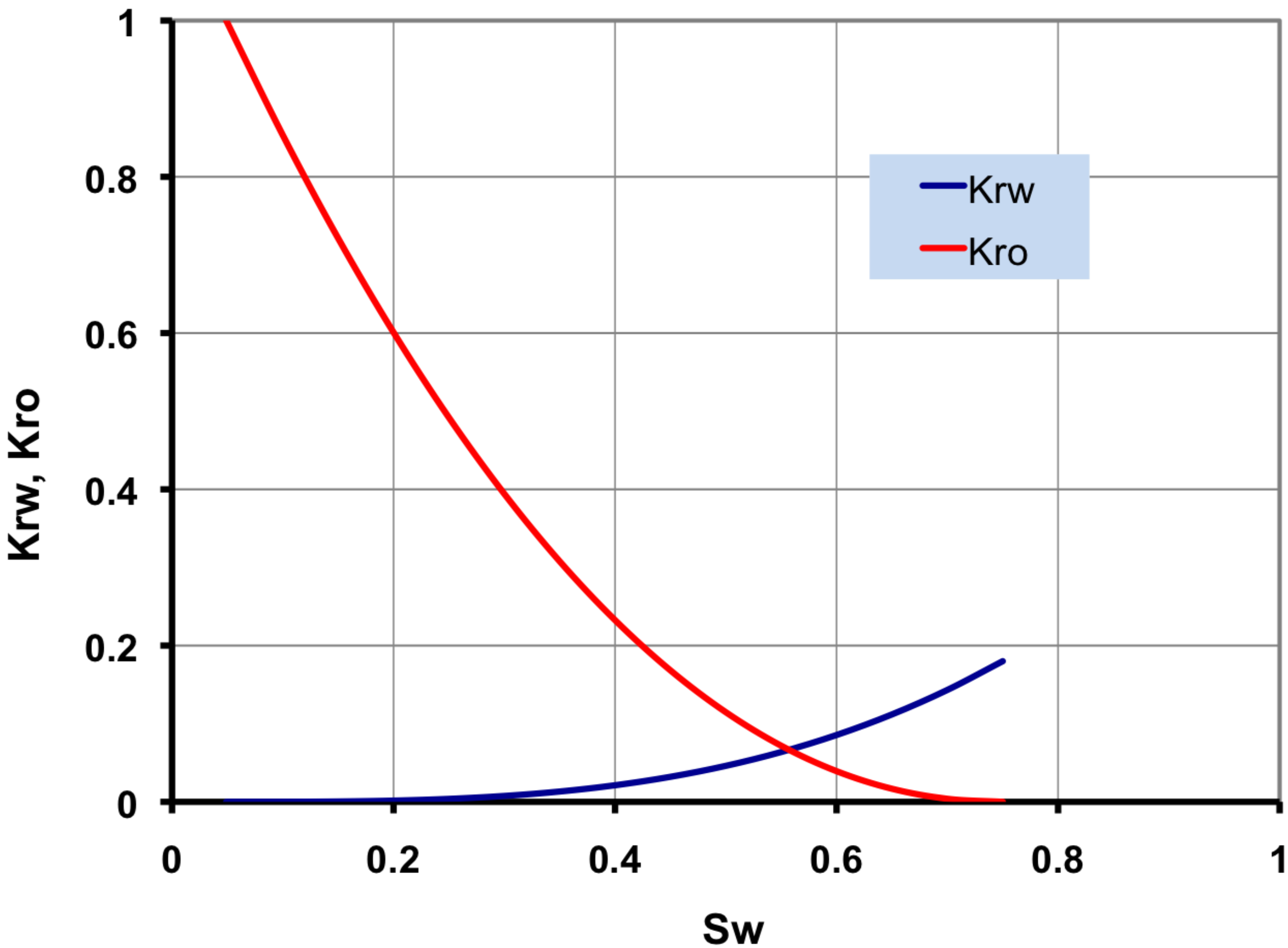

Permeability Distribution and Well Locations

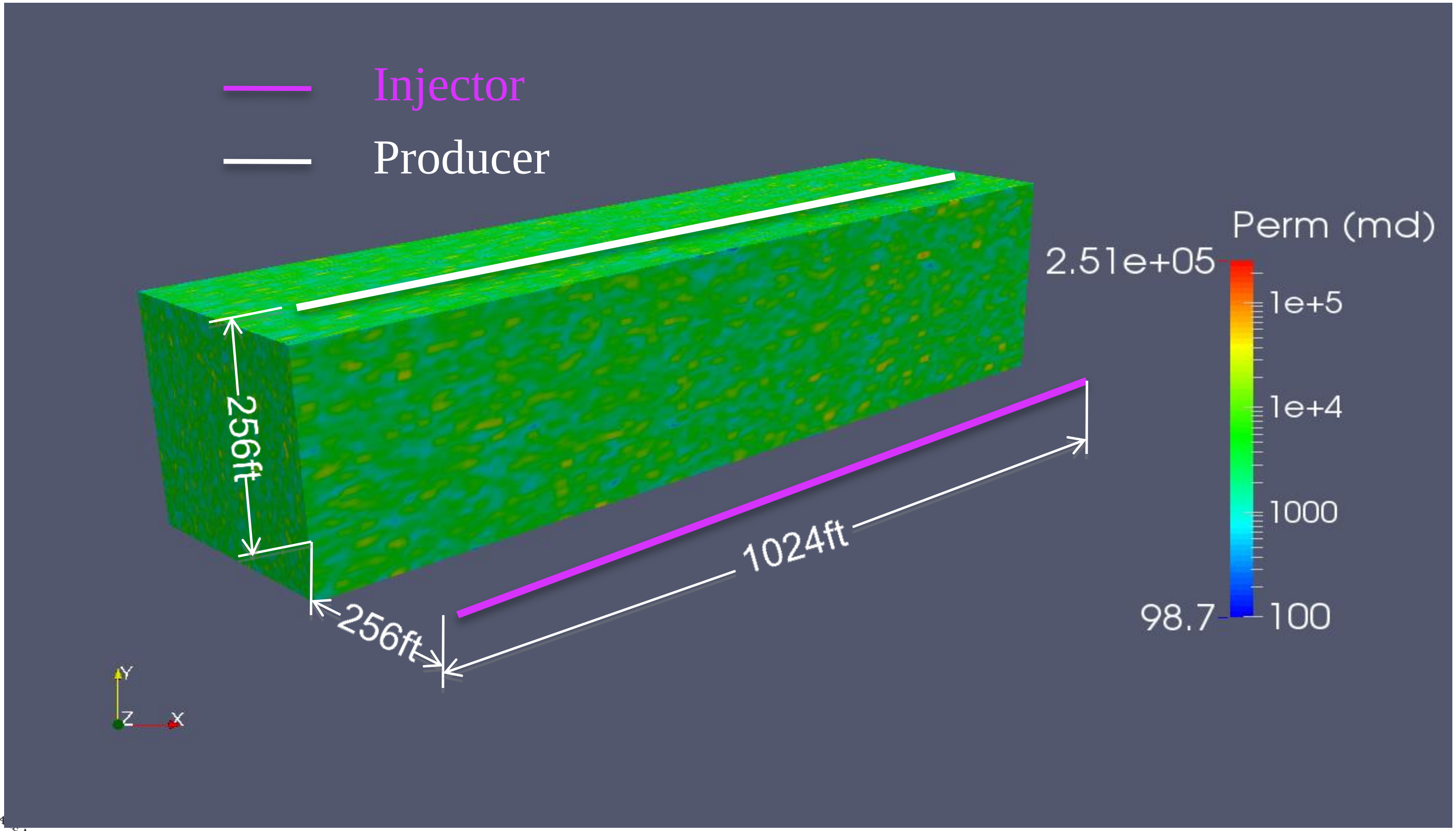

Simulation Results at 100 Day

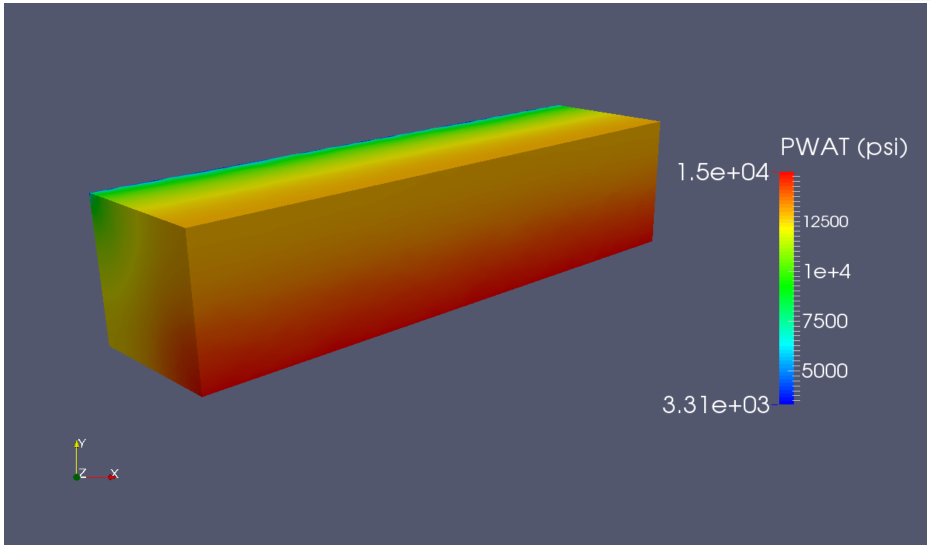

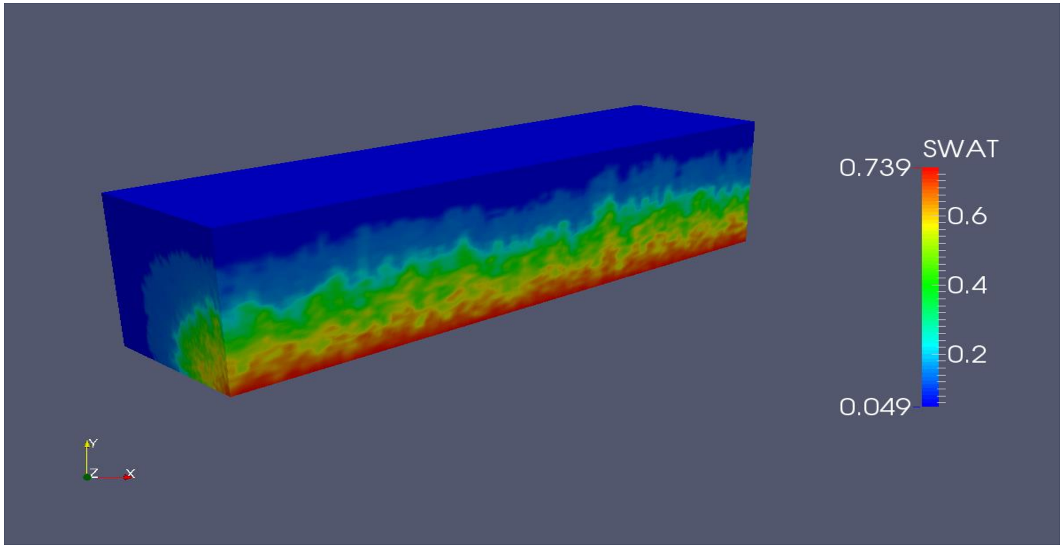

Simulation Results at 100 Day (Cont.)

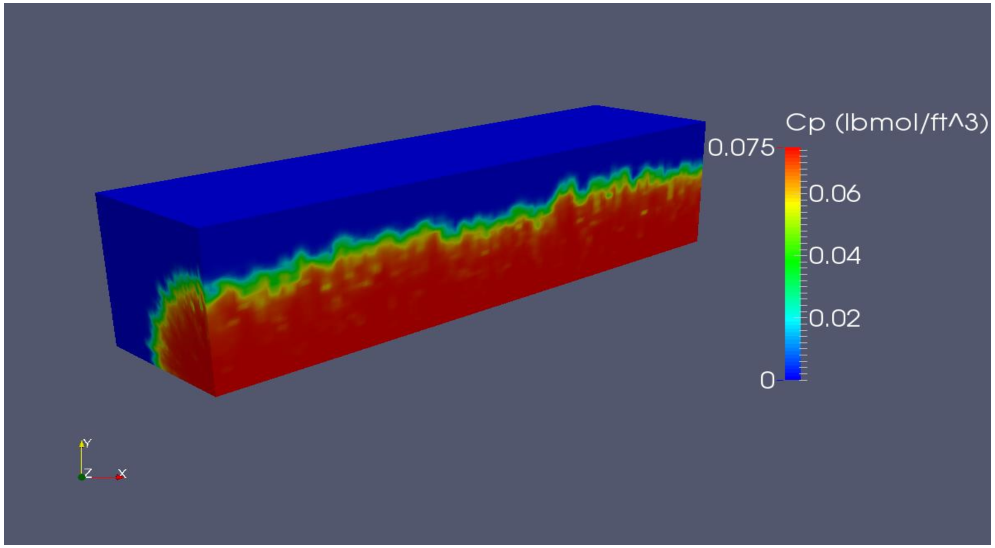

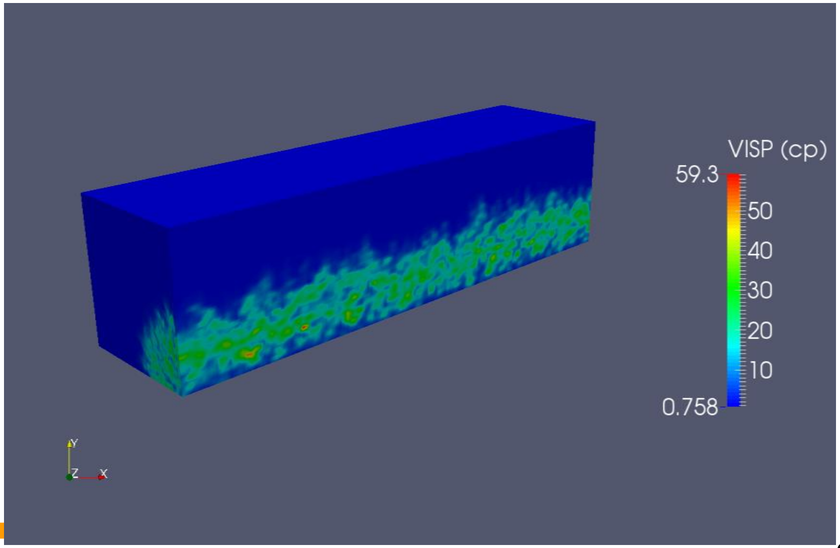

Compositional Equations

Component Conservation Equation

$$\frac{\partial}{\partial t}\left(\sum_\alpha \phi S_\alpha \rho_\alpha \xi_{i\alpha}\right) + \nabla \cdot \sum_\alpha \left(\rho_\alpha \xi_{i\alpha} \boldsymbol{u}_\alpha - \phi S_\alpha \boldsymbol{D}_{i\alpha} \cdot \nabla \left(\rho_\alpha \xi_{i\alpha}\right)\right) = \sum_\alpha q_{i\alpha}$$

Darcy Phase Flux

$$\boldsymbol{u}_\alpha = -\boldsymbol{K}\frac{k_{r\alpha}}{\mu_\alpha}\left(\nabla p_\alpha - \rho_\alpha g\right)$$

Define Component Flux

$$\boldsymbol{F}_i = -\boldsymbol{K}\left(\sum_\alpha \rho_\alpha \xi_{i\alpha}\frac{k_{r\alpha}}{\mu_\alpha}\left(\nabla p_{\text{ref}} - \rho_\alpha g\right) + \sum_{\alpha \neq \text{ref}} \rho_\alpha \xi_{i\alpha}\frac{k_{r\alpha}}{\mu_\alpha}\nabla p_{c\alpha}\right)$$

Modified Compositional Equations

$$\frac{\partial}{\partial t}\left(\phi N_i\right) + \nabla \cdot \boldsymbol{F}_i - \nabla \cdot \left(\sum_\alpha \phi S_\alpha \boldsymbol{D}_{i\alpha}\left(\nabla \rho_\alpha \xi_{i\alpha}\right)\right) = q_i$$

Closure & Constraints

Capillary Pressure

$$p_{c\alpha} = p_\alpha - p_{\text{ref}}$$

Phase Behavior

$$\rho_\alpha = \frac{p_\alpha}{Z_\alpha RT}$$

$$\rho_w = \rho_{w,0} exp\left[C_w(p_{\text{ref}} + p_{cw} - p_{\text{ref,std}})\right]$$

Rock Compressibility

$$\phi = \phi_0 \left[1 + C_r(p_{\text{ref}} - p_{\text{ref,std}})\right]$$

Saturation Constraint

$$\sum_\alpha S_\alpha = 1$$

$$S_w = \frac{N_w}{\rho_w}$$

$$S_o = \frac{(1-\nu)}{\rho_o} \sum_{i=2}^{N_c} N_i$$

$$S_g = \frac{\nu}{\rho_g} \sum_{i=2}^{N_c} N_i$$

Hydrocarbon Phase Behavior

Peng-Robinson Cubic EOS

$$\bar{Z}_\alpha^3 - (1 - B_\alpha)\bar{Z}_\alpha^2 + \left(A_\alpha - 3B_\alpha^2 - 2B_\alpha\right)\bar{Z}_\alpha - \left(A_\alpha B_\alpha - B_\alpha^2 - B_\alpha^3\right) = 0$$

$$Z_\alpha = \bar{Z}_\alpha - C_\alpha$$

Rachford-Rice for phase mole fraction (*ν*)

$$f = \sum_{i=2}^{N_c} \frac{(K_i^{\text{par}} - 1)z_i}{1 + (K_i^{\text{par}} - 1)\nu} = 0$$

Iso-fugacity criteria for K_i^{par}

$$g = ln(\Phi_{io}) - ln(\Phi_{ig}) - lnK_i^{\text{par}} = 0$$

Gibbs energy minimization for phase stability

$$dG|_{\alpha,T,P} = \sum_{i=2}^{N_c} \left.\frac{\partial G}{\partial n_i}\right|_{\alpha,T,P} dn_i = h(Z_\alpha)$$

Discrete Form

Component Flux

$$\left\langle \frac{1}{\Lambda_{i,h}^{\tilde{k}}} \boldsymbol{K}^{-1} \boldsymbol{F}_{i,h}^{k+1}, v_h \right\rangle_{Q,E} - \left(p_{\mathrm{ref},h}^{k+1}, \nabla \cdot v_h\right)_E = -\int_{\partial E \cap \partial \Omega} p_{\mathrm{ref}} v_h \cdot n - \left(\frac{1}{\Lambda_{i,h}^{\tilde{k}}} \sum_{\alpha \neq \mathrm{ref}} \rho_{\alpha,h}^{\tilde{k}} \xi_{i\alpha,h}^{\tilde{k}} \lambda_{\alpha,h}^{\tilde{k}} \nabla p_{c\alpha,h}^{\tilde{k}}, v_h\right)_E + \left(\frac{1}{\Lambda_{i,h}^{\tilde{k}}} \sum_{\alpha} \left(\rho_{\alpha,h}^{2}\right)^{\tilde{k}} \xi_{i\alpha,h}^{\tilde{k}} g, v_h\right)_E,$$

Component Conservation Equation

$$\left(\frac{\phi_h^{k+1} N_{i,h}^{k}}{\Delta t}, w_h\right)_E + \left(\nabla \cdot \boldsymbol{F}_{i,h}^{k+1}, w_h\right)_E - \left(\nabla \cdot \sum_{\alpha} \left\{\phi_h^{k+1} S_{\alpha,h}^{\tilde{k}} \boldsymbol{D}_{i\alpha,h} \cdot \nabla \left(\rho_{\alpha,h}^{\tilde{k}} \xi_{i\alpha,h}^{\tilde{k}}\right)\right\}, w_h\right)_E = \left(q_{i,h}^{\tilde{k}}, w_h\right) + \left(\frac{\phi^n N_i^n}{\Delta t}, w_h\right)_E.$$

- Enhanced BDDF_1 mixed finite element space
- Symmetric and non-symmetric quadrature rules (Q)
- 9 and 27 point stencil for 2 and 3 dimensions, respectively
- Λ_is are positive quantities

Diffusion-Dispersion

Full Tensor Diffusion-Dispersion

$$\boldsymbol{D}_{i\alpha} = \boldsymbol{D}_{i\alpha}^{\text{mol}} + \boldsymbol{D}_{i\alpha}^{\text{hyd}}$$

$$\boldsymbol{D}_{i\alpha}^{\text{mol}} = \tau_\alpha d_{m,i\alpha} \boldsymbol{I}$$

$$\boldsymbol{D}_{i\alpha}^{\text{hyd}} = d_{t,\alpha} |\boldsymbol{v}_\alpha| \boldsymbol{I} + \left(d_{l,\alpha} - d_{t,\alpha}\right) \boldsymbol{v}_\alpha \boldsymbol{v}_\alpha^T / |\boldsymbol{v}_\alpha|$$

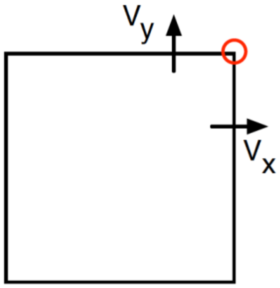

Diffusive-Dispersive Flux Calculation

$$\boldsymbol{J}_{i\alpha} = \phi S_\alpha \boldsymbol{D}_{i\alpha} \rho_\alpha \cdot \nabla \left(\xi_{i\alpha}\right),$$

$$\left\langle \frac{1}{\phi \rho_\alpha S_\alpha} \boldsymbol{D}_{i\alpha}^{-1} \boldsymbol{J}_{i\alpha}, v_h \right\rangle_{Q,E} - \left(\xi_{i\alpha}, \nabla \cdot v_h\right)_E = - \int_{\partial E \cap \partial \Omega} \xi_{i\alpha} v_h \cdot n.$$

- Accurate dispersion tensor calculation using flux vector at each corner
- Reduced grid-orientation effect on concentrations

Linearized Form

Component Flux

$$\left\langle \frac{1}{\Lambda_{i,h}} K^{-1} \delta \boldsymbol{F}_{i,h}, v_h \right\rangle_{Q,E} - \left(\delta p_{\text{ref},h}, \nabla \cdot v_h\right)_E = -R_{3i}$$

Component Mass Conservation

$$\left(\frac{\phi_h^{n+1,k} \delta N_{i,h}}{\Delta t}, w_h \right)_E + \left(\frac{N_{i,h}^{n+1,k}}{\Delta t} \frac{\partial \phi}{\partial p_{\text{ref},h}} \delta p_{\text{ref},h}, w_h \right)_E + \left(\nabla \cdot \delta \boldsymbol{F}_{i,h}, w_h\right)_E = -R_{4i}$$

$$\begin{pmatrix} A_i & B & 0 \\ B^T & C_i & D_i \end{pmatrix} \begin{pmatrix} \boldsymbol{\delta F_i} \\ \boldsymbol{\delta p_{\text{ref}}} \\ \boldsymbol{\delta N_i} \end{pmatrix} = \begin{pmatrix} -\boldsymbol{R}_{3i} \\ -\boldsymbol{R}_{4i} \end{pmatrix}$$

- Eliminate fluxes δF_i to obtain a linear system of equations in δP and δN_i

Linearized Form

Saturation Constraint

$$\sum_\alpha \frac{\partial S_\alpha}{\partial p_{\text{ref}}}\delta p_{\text{ref}} + \sum_\alpha \sum_i \frac{\partial S_\alpha}{\partial N_i}\delta N_i + \sum_\alpha \sum_i \frac{\partial S_\alpha}{\partial ln K_i^{\text{par}}}\delta ln K_i^{\text{par}} + \sum_\alpha \frac{\partial S_\alpha}{\partial \nu}\delta \nu = 1 - \sum_\alpha S_\alpha = -R_5$$

Fugacities at Equilibrium

$$\frac{\partial ln\Phi_{io}}{\partial p_{\text{ref}}}\delta p_{\text{ref}} + \sum_{k=2}^{N_c} \frac{\partial ln\Phi_{io}}{\partial N_k}\delta N_k + \sum_{k=2}^{N_c} \frac{\partial ln\Phi_{io}}{\partial ln K_k^{\text{par}}}\delta ln K_k^{\text{par}} + \frac{\partial ln\Phi_{io}}{\partial \nu}\delta\nu - \left(\frac{\partial ln\Phi_{ig}}{\partial p_{\text{ref}}}\delta p_{\text{ref}} \right.$$
$$\left. + \sum_{k=2}^{N_c} \frac{\partial ln\Phi_{ig}}{\partial N_k}\delta N_k + \sum_{k=2}^{N_c} \frac{\partial ln\Phi_{ig}}{\partial ln K_k^{\text{par}}}\delta ln K_k^{\text{par}} + \frac{\partial ln\Phi_{ig}}{\partial \nu}\delta\nu\right) - \frac{\partial ln K_i^{\text{par}}}{\partial ln K_k^{\text{par}}}\delta ln K_k^{\text{par}} = -R_{6i}$$

$$\begin{pmatrix} E & F & G & H \\ I & J & K & L \\ 0 & N & O & P \end{pmatrix} \begin{pmatrix} \delta p_{\text{ref}} \\ \boldsymbol{\delta N} \\ \boldsymbol{\delta ln K}^{\text{par}} \\ \boldsymbol{\delta\nu} \end{pmatrix} = \begin{pmatrix} -\boldsymbol{R}_5 \\ -\boldsymbol{R}_6 \\ -\boldsymbol{R}_7 \end{pmatrix}$$

- Eliminate fluxes δK^{par} and δv to obtain a linear system of equations in δP and δN_i

Brugge Field Study

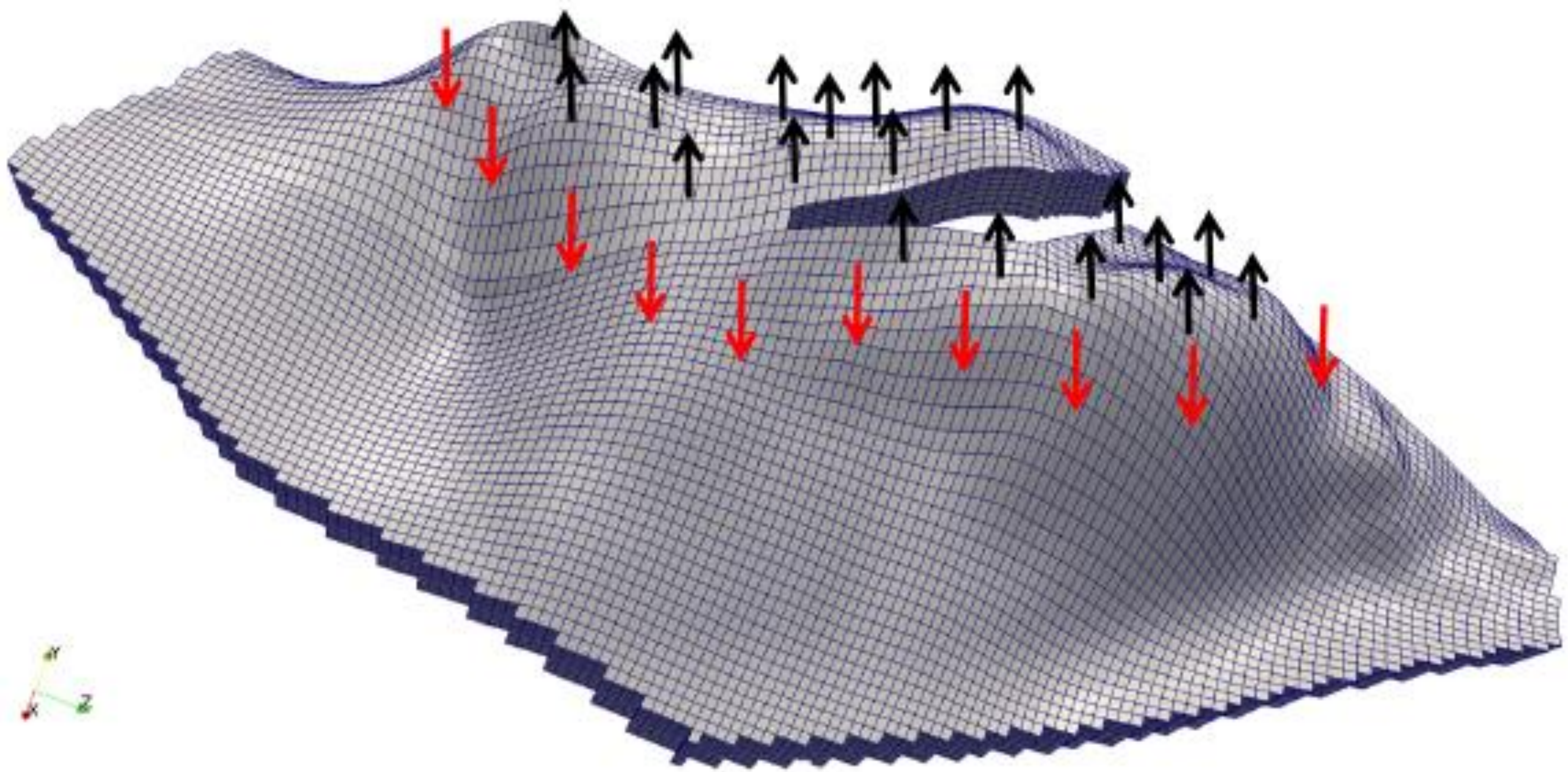

Brugge field geometry and well locations

Reservoir Properties

- 9x48x139 general hexahedral elements
- In-situ hydrocarbon fluid composition: 40% C_6, 60% C_{20}
- Injected fluid composition: 100 % CO_2
- Initial reservoir pressure: 1500 psi
- 30 bottom-hole pressure specified wells
  - 10 injectors at 3000 psi
  - 20 producers at 1000 psi
- Initial water saturation: $S_w = 0.2$
- $\varphi \approx 0.14 - 0.24$, $K_z = K_y$, $T_{res} = 160$ F

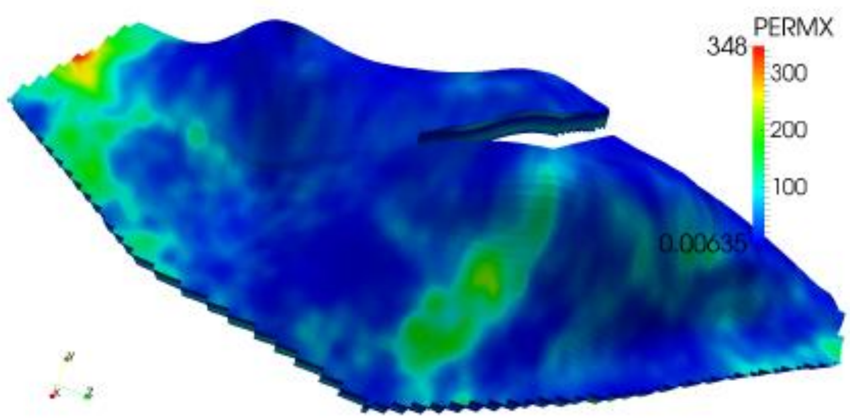

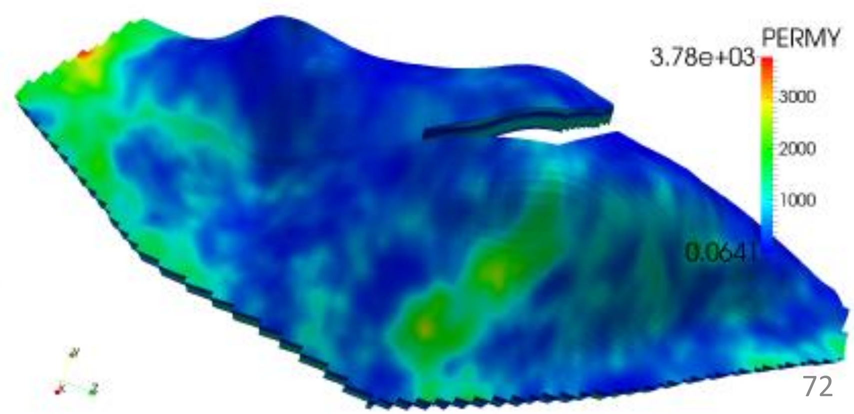

Rock Properties

Relative Permeability Curves

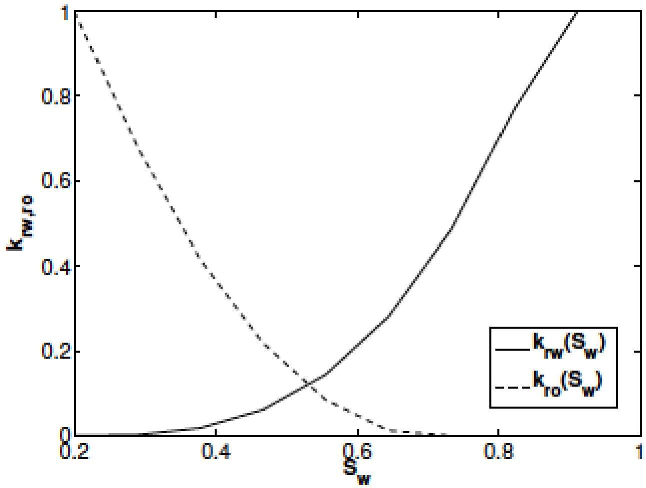

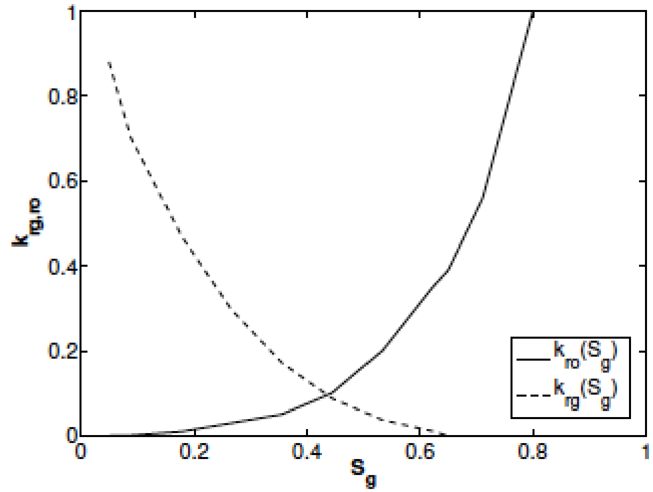

Capillary Pressure Curves

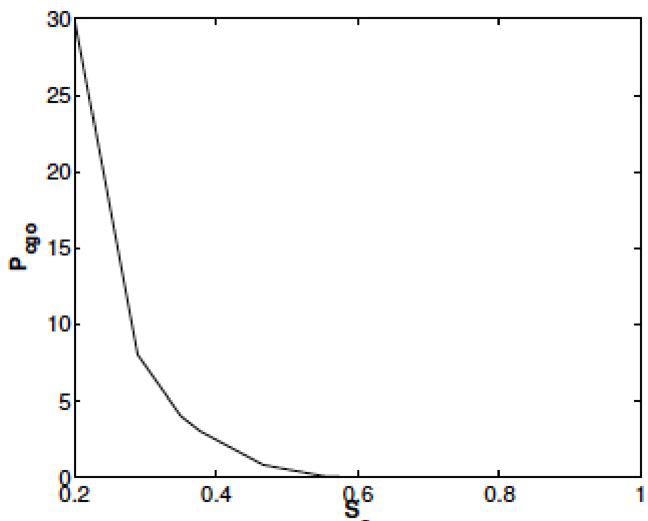

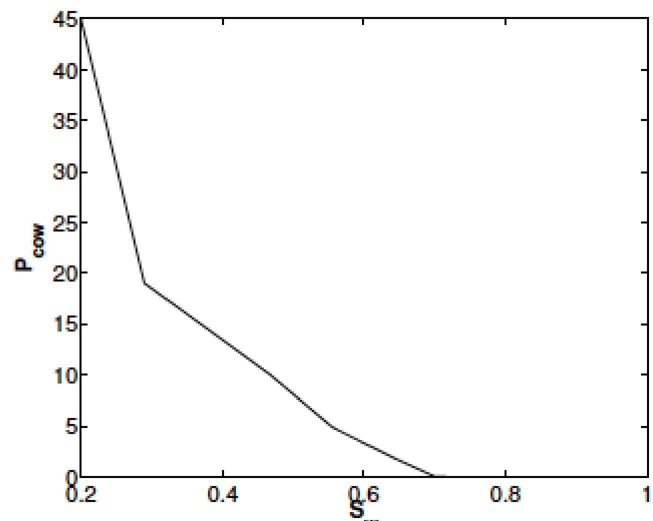

Pressure & Concentration Profiles

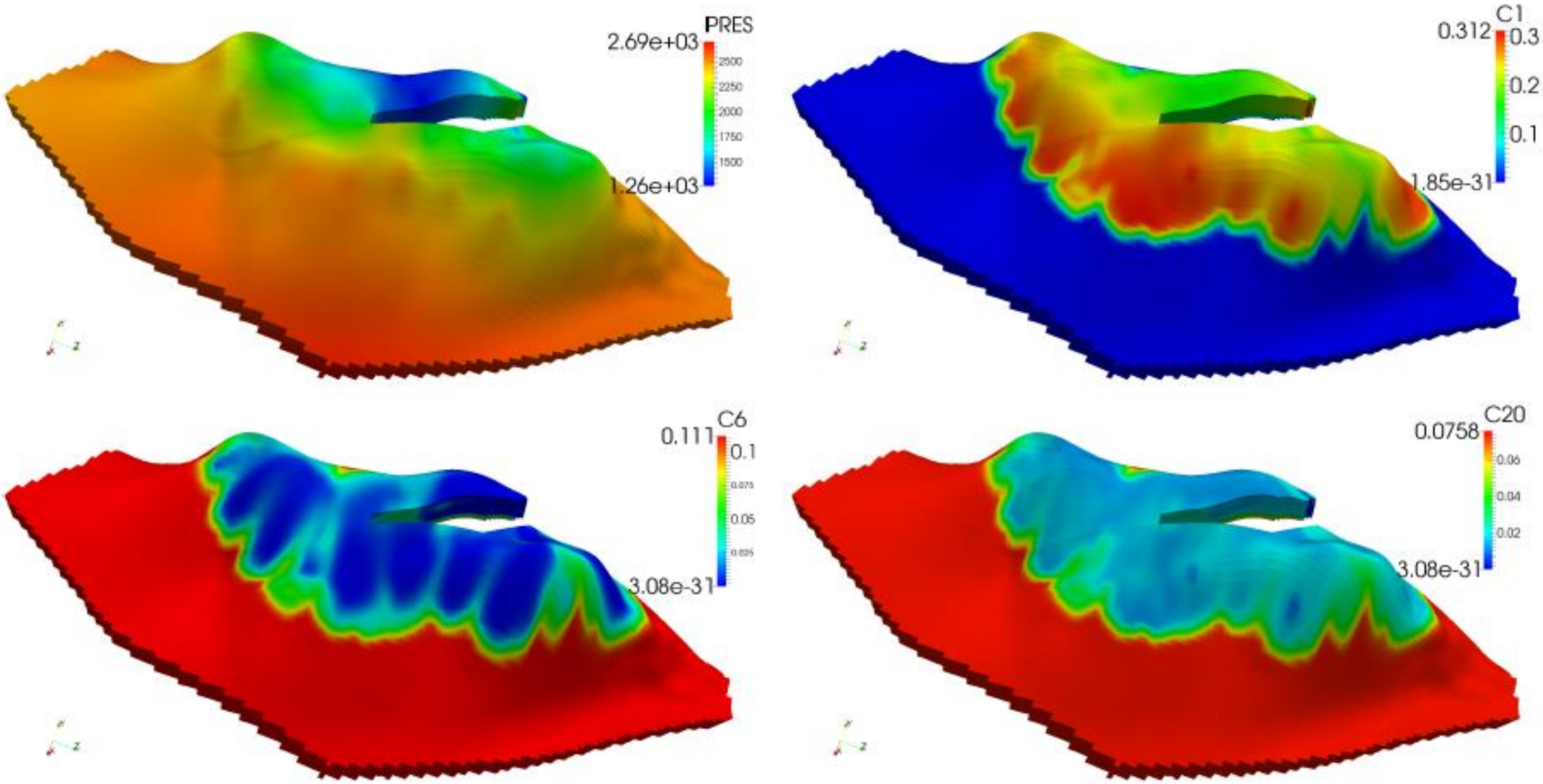

Pressure and concentration profiles after 1000 days

Saturation Profiles

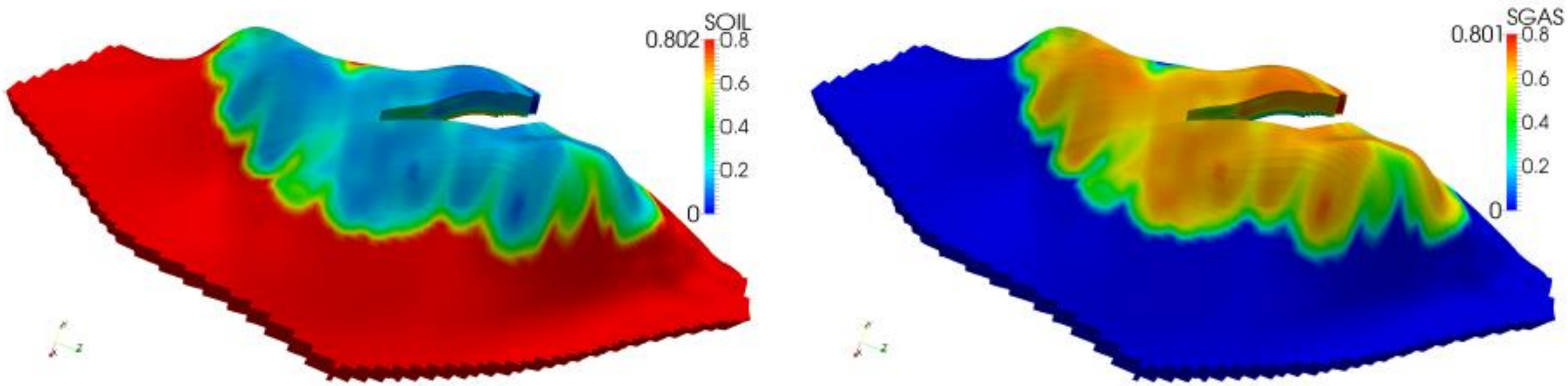

Saturation profiles after 1000 days

- Multi-contact miscible flood
- Miscibility achieved at the tail end of the displacement front

Hydraulic Fracturing Stages

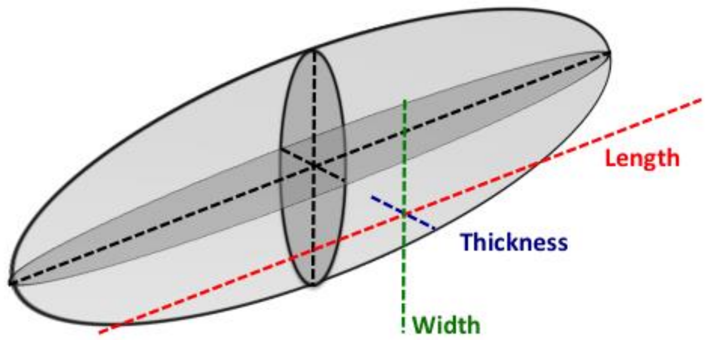

- Fracture growth: slick water injection
  - Length
- Proppant placement: polymer injection
  - Width due to polymer injection
  - Thickness due to proppant
- Compaction

Proppant Placement

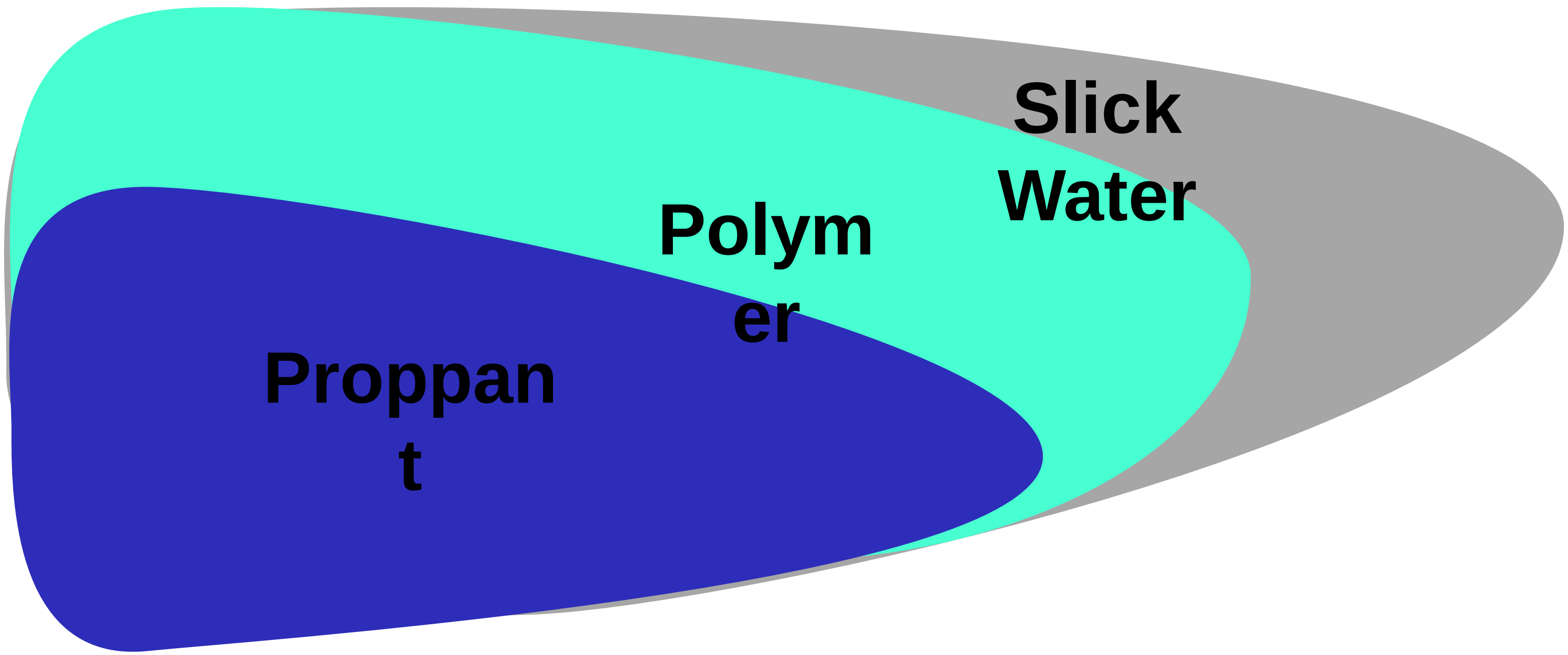

Well Model Updates

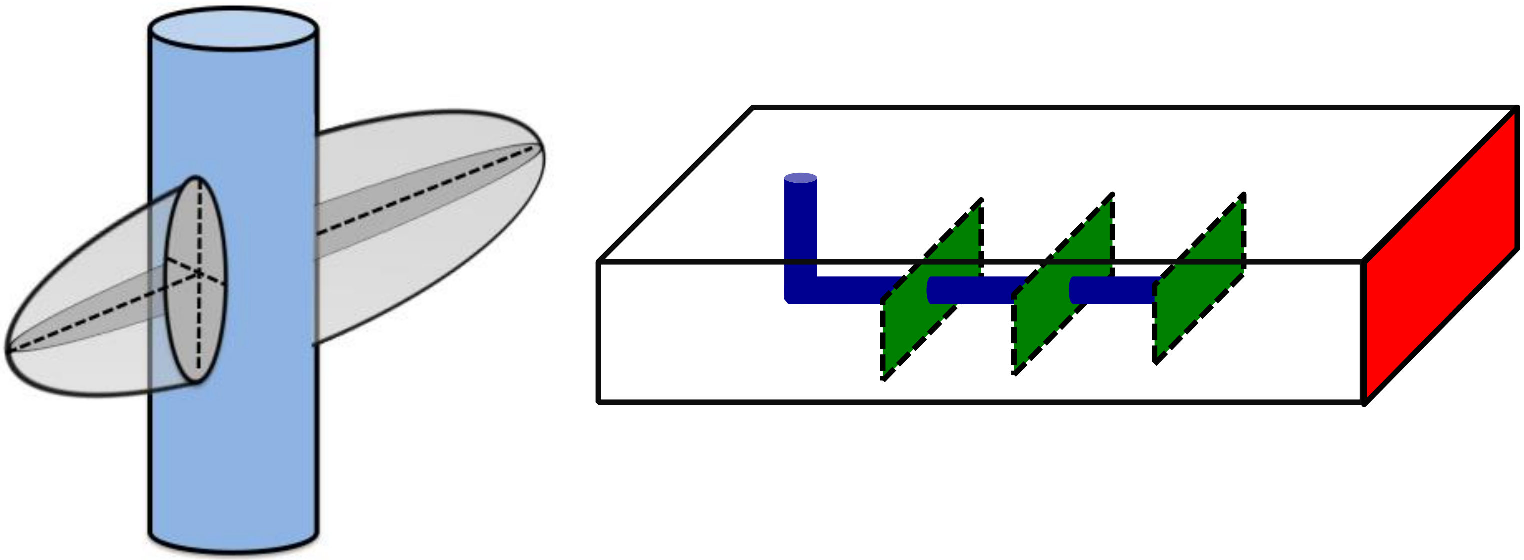

- Multistage hydraulic fractures in a single well bore

Characteristics

- Polymer front travels ahead of proppant front
- Initial fracture thickness due to fracture growth during slick water injection
- Intermediate thickness increase due to fluid pressure front ahead of proppant front
- Final thickness related to proppant concentration
- Compaction related width changes

Phase Field for Crack Propagation (Mikelic, W, Wick)

Four advantages

- Fixed-mesh approach avoiding remeshing
- Crack nucleation, propagation and path are included in the model avoiding evaluation of stress intensity factors
- Joining and branching of multiple cracks easy to realize
- Cracks in heterogeneous media

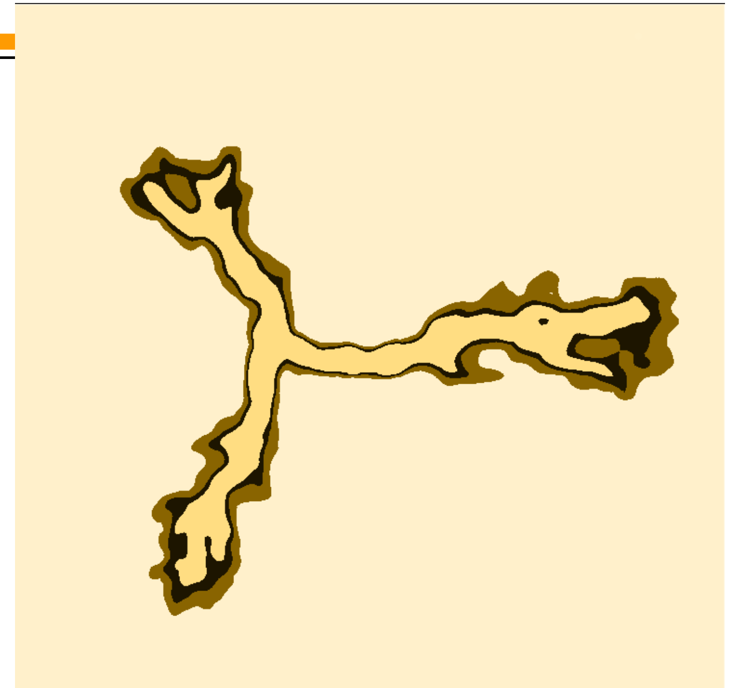

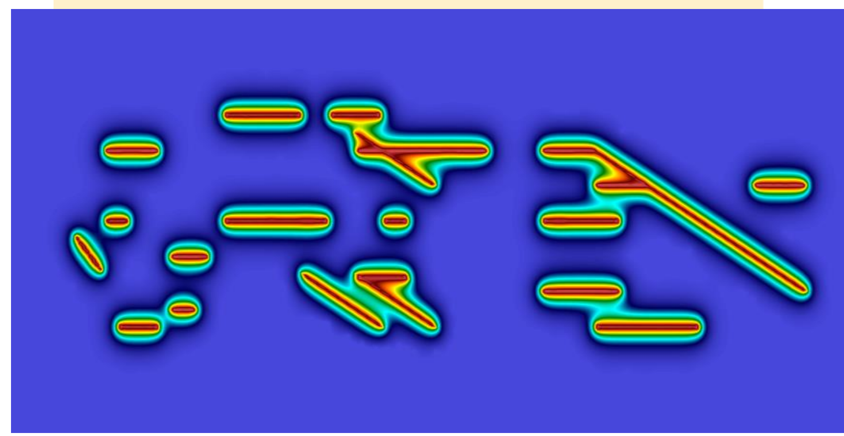

Energized Fractures

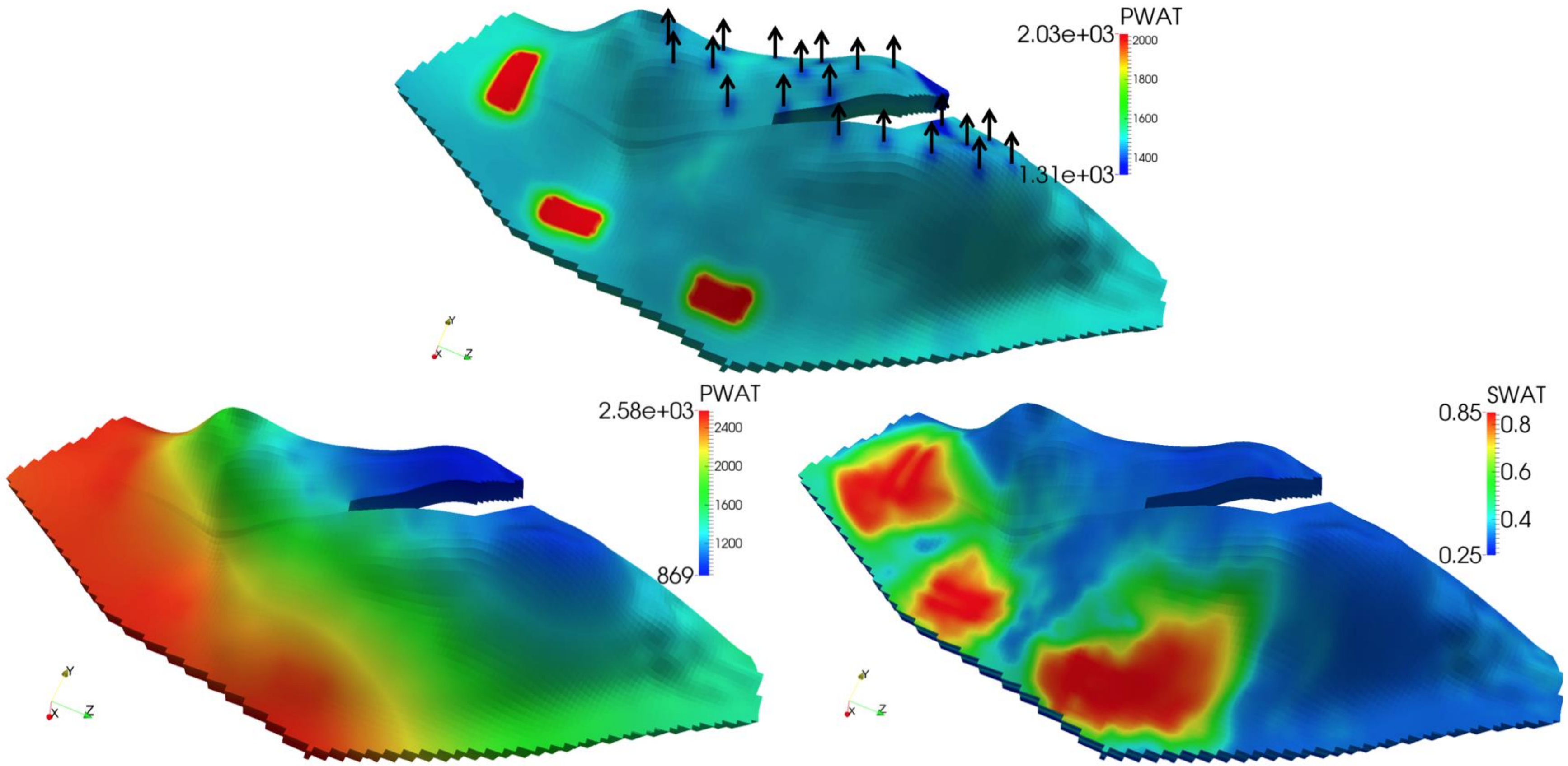

In Salah Reservoir

- Salah Gas Project in Algeria is world's first industrial scale CO_2 storage project in depleting gas field
- Aprox. 0.5-1 M tons CO_2 per year injected since August 2004
- Aquifer: low-permeability, 20 m thick carboniferous sandstone, 1800-1900 m deep

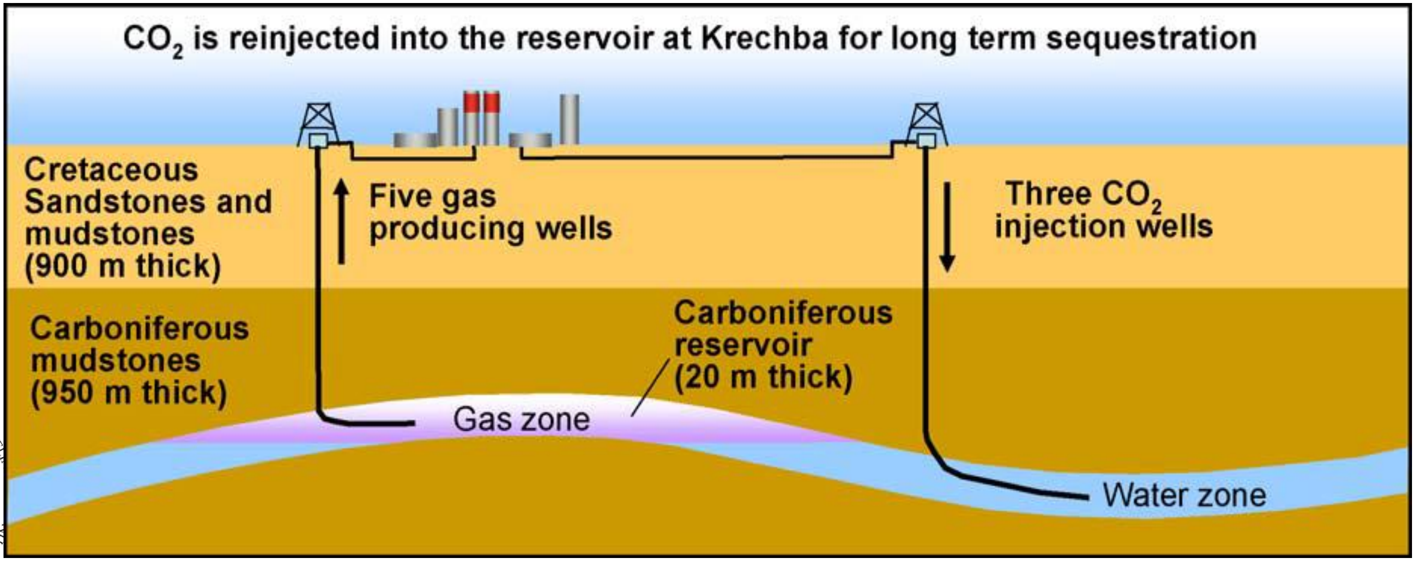

Schematic vertical cross section through the Krechba field (Rutqvist

In Salah Reservoir

- Three long-reach (about 1-1.5 km) horizontal injection wells
- Satellite-based inferrometry (InSAR) has been used for detecting ground surface deformations related to the CO2 injection
- Uplift occurred within a month after start of the injection and the rate of uplift was approximately 5 mm per year (~2 cm for 4 years over the injection wells)

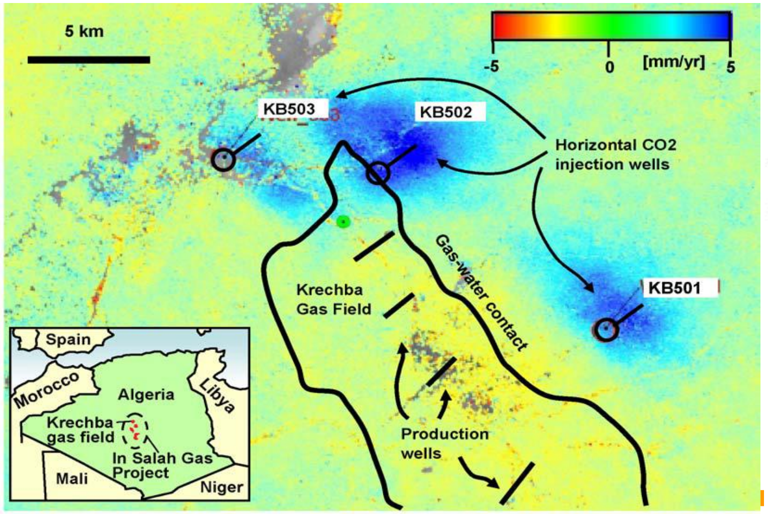

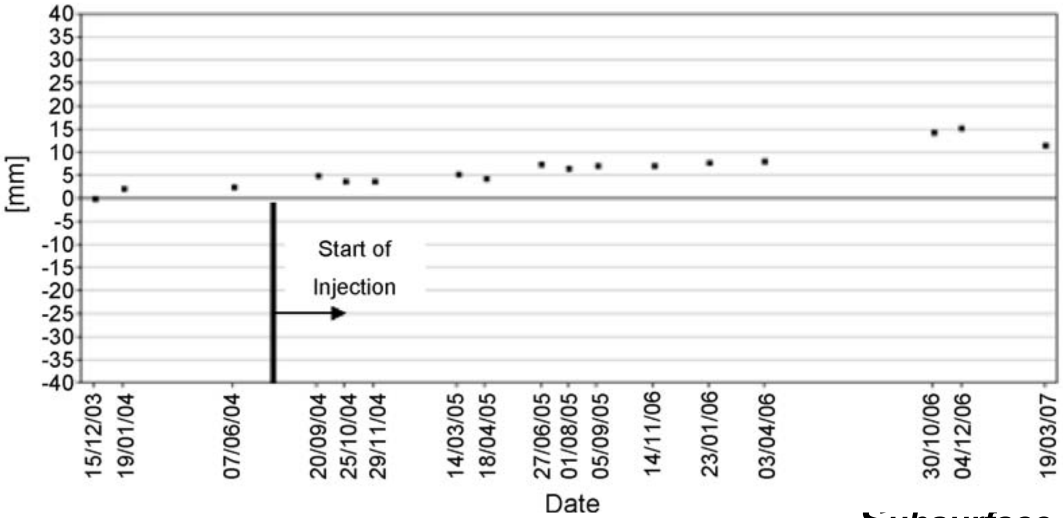

Vertical displacements at 3 years (left) and time evolution of vertical displacement for a location above KB501 (right) (Rutqvist et al., 2009)

In Salah Reservoir

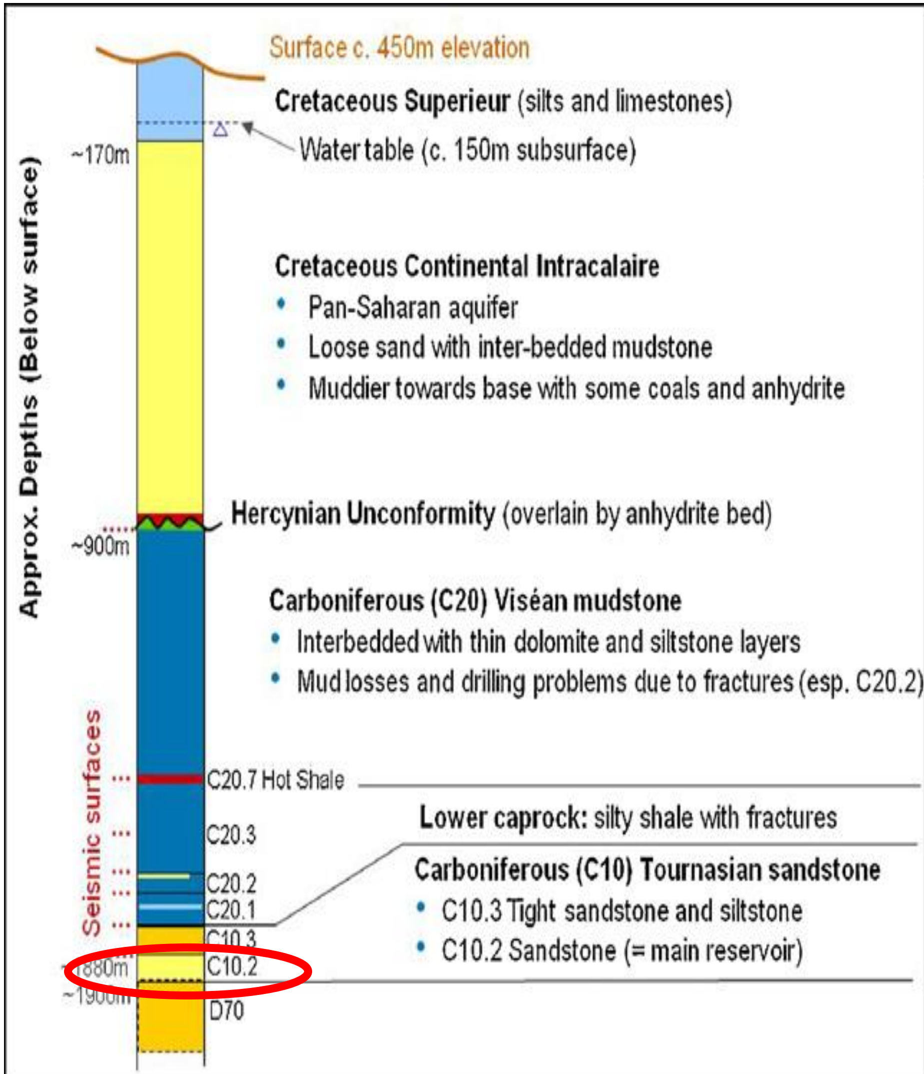

After Ringrose (2007)

- **The main CO2 storage aquifer (C10.2) is approximately 20–25m thick.**
- **The C10.2 formation is overlain by a tight sandstone and siltstone formation (C10.3) of about 20m in thickness.**
- **The C10 formation, together with the lower cap rock (C20.1–C20.3), form the CO2 storage complex at Krechba.**
- **It has been shown that most of the observed uplift may be attributed to the poroelastic expansion of the 20m thick storage formation, but a significant contribution could come from pressure-induced deformation within a larger zone (~100m thick) of shale sands immediately above the injection zone (Rutqvist et al. (2009)).**

Geomechanic Domain

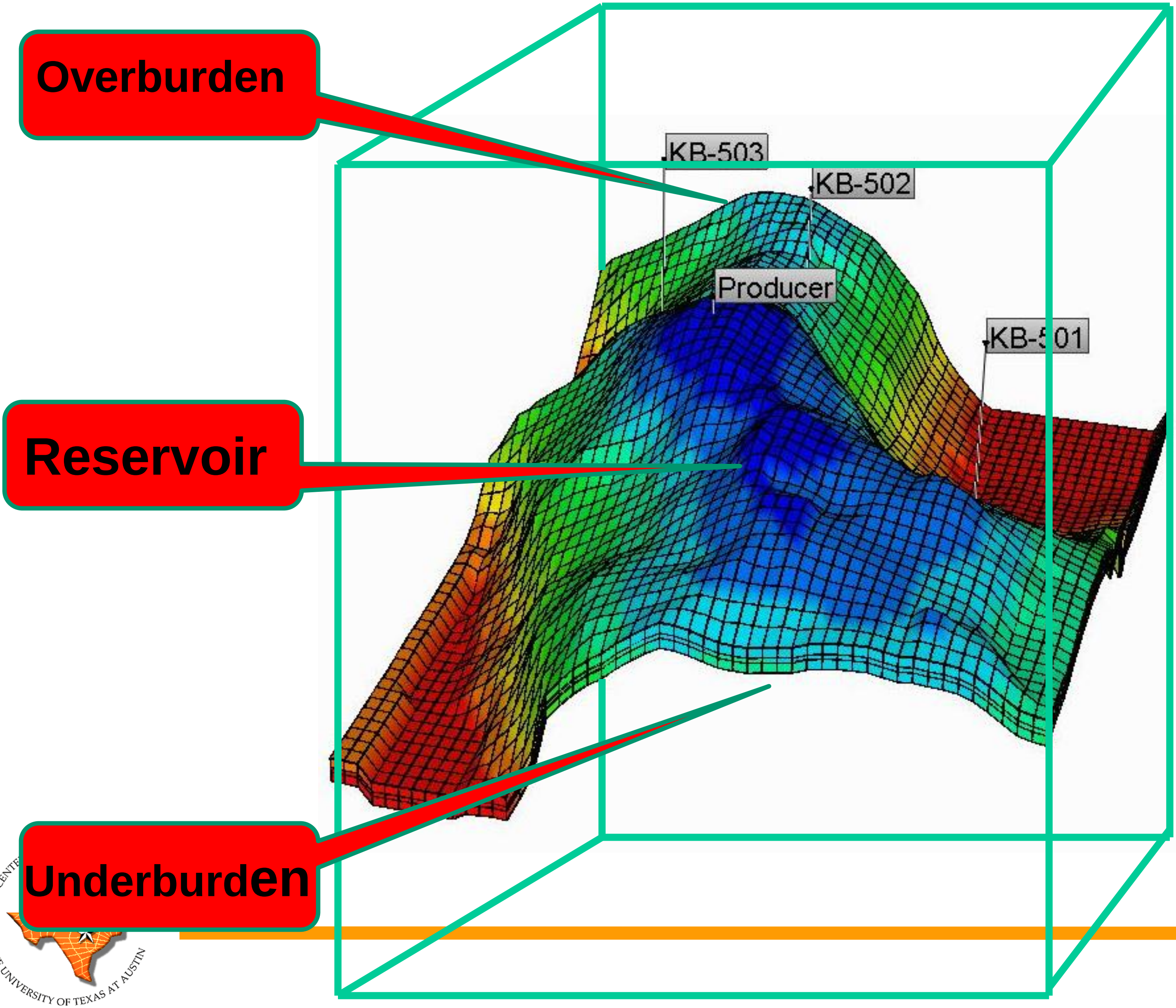

Summary

- Dynamic flow data (BHP and CO2 saturation) and surface deformation very sensitive to geomechanical properties of the formation such as Young's modulus and Poisson ratio. Reservoir traction an important source of uncertainty in injection and production data.

- Integration of geomechanical observed data in addition to flow data should be considered for better reservoir characterization.

- Future plan: Full field reservoir simulation and characterization of In Salah reservoir using observed data from three injection wells and surface uplift InSAR data.

Conclusions

- General hexahedral elements to handle complex reservoir geometries
- Full tensor permeability and dispersion
- Locally mass conservative and accurate flux description
- Reduced grid orientation effect on pressure and concentration
- Integration of single, two, black oil, and compositional formulations under a single MFMFE framework
- Extension to coupled ASP and/or compositional flow and geomechanics for fractured reservoirs
- Coupling with phase field for fracture propagation